Alzheimer's Research & Therapy

RESEARCH

Open Access

Photobiomodulation modulates mitochondrial energy metabolism and ameliorates neurological damage in an APP/PS1 mousmodel of Alzheimer's disease

Hongli Chen[1,2,3*], Na Li[1,2], Na Liu[2,3], Hongyu Zhu[2], Chunyan Ma[1,2], Yutong Ye[1,2], Xinyu Shi[2], Guoshuai Luo[4], Xiaoxi Dong[1], Tao Tan[5], Xunbin Wei[6*] and Huijuan Yin[1*]

Abstract

Background Alzheimer's disease (AD) is a neurodegenerative disease. Amyloid β-protein (Aβ) is one of the key pathological features of AD, which is cytotoxic and can damage neurons, thereby causing cognitive dysfunction. Photobiomodulation (PBM) is a non-invasive physical therapy that induces changes in the intrinsic mechanisms of cells and tissues through low-power light exposure. Although PBM has been employed in the treatment of AD, the effect and precise mechanism of PBM on AD-induced neurological damage are still unclear.

Methods In vivo experiments, PBM (808 nm, 20 mW/cm^2) was used to continuously interfere with APP/PS1 mice for 6 weeks, and then their cognitive function and AD pathological changes were evaluated. In vitro experiments, lipopolysaccharide (LPS) was used to induce microglia to model inflammation, and the effect of PBM treatment on microglia polarization status and phagocytic Aβ ability was evaluated. Hexokinase 2 (HK2) inhibitor 3-bromopyruvate (3BP) was used to study the effect of PBM treatment on mitochondrial energy metabolism in microglia.

Results PBM further ameliorates AD-induced cognitive impairment by alleviating neuroinflammation and neuronal apoptosis, thereby attenuating nerve damage. In addition, PBM can also reduce neuroinflammation by promoting microglial anti-inflammatory phenotypic polarization; Promotes Aβ clearance by enhancing the ability of microglia to engulf Aβ. Among them, PBM regulates microglial polarization and inhibits neuronal apoptosis, which may be related to its regulation of mitochondrial energy metabolism, promotion of oxidative phosphorylation, and inhibition of glycolysis.

Conclusion PBM regulates neuroinflammatory response and inhibits neuronal apoptosis, thereby repairing Aβ-induced neuronal damage and cognitive dysfunction. Mitochondrial energy metabolism plays an important role

*Correspondence:
Hongli Chen
chenhli0107@163.com
Xunbin Wei
xwei@bjmu.edu.cn
Huijuan Yin
yinzi490@163.com
Full list of author information is available at the end of the article

in PBM in improving nerve injury in AD mice. This study provides theoretical support for the subsequent application of PBM in the treatment of AD.

Keywords Alzheimer's disease, Photobiomodulation, Mitochondrial energy metabolism, Microglia, Apoptosis

Introduction

Alzheimer's disease (AD) is an irreversible neurodegenerative disease, characterised by impaired cognition, memory loss, decreased comprehension and expression, anxiety and depression [1]. The principal pathological characteristics of AD include the formation of senile plaques resulting from the aggregation of amyloid β-protein (Aβ) and neurofibrillary tangles, which leads to mitochondrial dysfunction, neuroinflammation, and neuronal damage [2, 3]. Neuronal damage represents a significant pathological manifestation of AD and an important etiological factor that mediates cognitive function and anxiety-like behaviours in AD [4, 5]. Aβ induces neuronal apoptosis by interfering with the endogenous mitochondrial pathway by mediating oxidative stress and cytochrome *C* (Cytc) release through ring-breaking mitochondrial function, and by activating caspase proteins, which leads to neuronal apoptosis [6]. The polarisation of microglia exacerbates neuroinflammation and impairs Aβ clearance, which precipitates neuronal damage and accelerating the progression of AD [7, 8].

Photostimulation has been shown to have the potential as a non-invasive intervention to ameliorate AD. It has been demonstrated to alleviate pathological and cognitive dysfunction in animal models of AD [9, 10]. Photobiomodulation (PBM) is a non-invasive approach to physical therapy that alters the intrinsic mechanism of cells or tissues [11]. PBM can reduce the level of Aβ plaques in the central nervous system (CNS) via a range of mechanisms. Zhang et al. demonstrated that PBM can shift amyloid precursor protein (APP) processing to the non-amyloid production pathway and reduce Aβ production by activating the PKA/SIRT1 pathway [12]. Besides influencing the production of Aβ, PBM can also reduce Aβ plaques by prompting the body to clear Aβ [11]. It has been demonstrated that 1070 nm light can facilitate Aβ clearance by regulating microglial polarisation and improving the condition of AD mice by inhibiting endoplasmic reticulum stress through the secretion of exosomes [13, 14]. In addition, PBM can also affect mitochondrial function and neuroinflammation. Qiu et al. developed a method to control mitochondria-lysosomal contacts (MLCs) by optogenetics to induce mitochondrial fission with spatiotemporal precision [15]. And MLCs can be achieved blue-light-induced association mitochondria lysosomes through various photoactivatable dimerizers [15]. Eells et al. proposed that PBM should be used to treat diseases of tissue damage and mitochondrial dysfunction [16]. Begum et al. found that near-infrared light therapy increased ATP levels, reduced neuroinflammation, extends lifespan, and improves mobility in aged Drosophila melanogaster [17]. PBM can also protect retinal cells by reducing the number of macrophages and inflammatory markers by decreasing the expression of complement components, reducing the inflammatory response [18]. However, relatively few studies have been conducted around the effect of PBM on the pathological manifestations of AD (such as mitochondrial dysfunction, neuroinflammation, neuronal damage, etc.). Yang et al. demonstrated that PBM protects mitochondrial dynamics and improves mitochondrial function, slowing the progression of AD [19]. The regulation of mitochondrial function by PBM may be a central mechanism in which it exerts a beneficial effect on AD.

The mitochondria play a pivotal role in the energy metabolism process of cells. Mitochondrial damage leads to an overproduction of reactive oxygen species (ROS) in cells, which in turn leads to oxidative damage, ultimately leading to cytotoxicity and cell death [20]. Mitochondrial dysfunction is a significant pathological phenomenon in AD [21]. Mitochondrial functions include biogenesis, energy metabolism, and autophagy [22, 23]. Mitochondrial energy metabolism is intimately linked to microglial polarisation and neuronal apoptosis. When Aβ deposition over-activates microglia, it prompts the conversion of mitochondrial oxidative phosphorylation (OXPHOS) metabolism to glycolysis, releasing large amounts of inflammatory factors and affecting phagocytosis [24]. Zhou et al. showed that Cornuside improves mitochondrial function by promoting OXPHOS and glycolysis, reducing ROS production and depolarization of mitochondrial membrane potential, thereby alleviating neuronal and synaptic damage, and ultimately improving cognitive function in AD mice [25]. Furthermore, Aβ has been shown to induce the release of Cytc from the mitochondrial electron transport chain, which disrupts mitochondrial energy metabolism and mediates apoptosis [26, 27]. One study showed that far-infrared light intervention could improve cognitive deficits in AD mice by enhancing Aβ clearance [28]. Wang et al. demonstrated that 808 nm near-infrared (NIR) light promoted lymphatic drainage, reducing Aβ load by regulating mitochondrial energy metabolism in meningeal lymphatic endothelial cells [29]. Although numerous studies have demonstrated

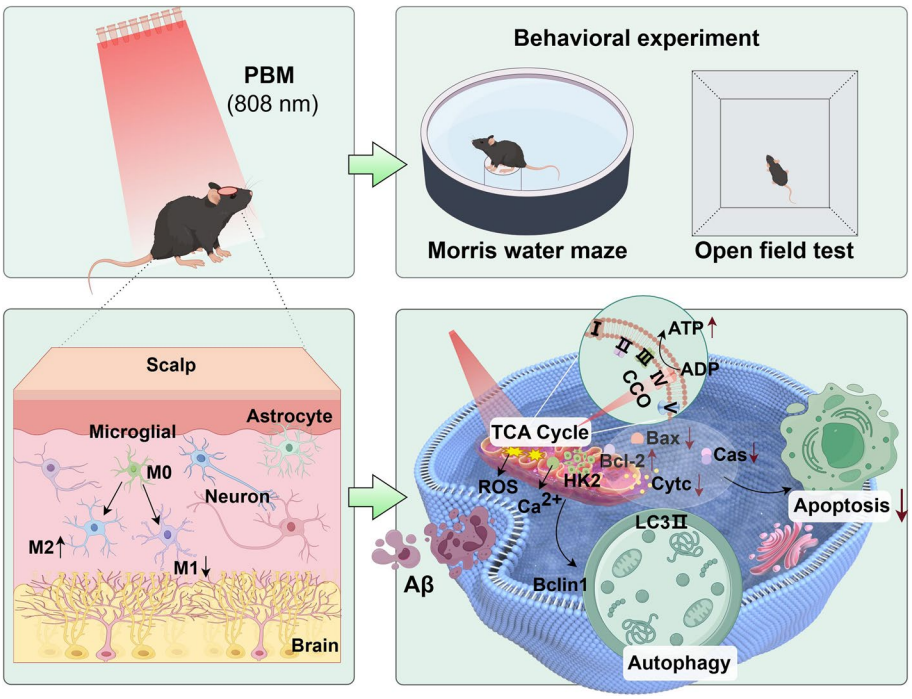

Scheme 1 Schematic illustration of the mechanism by Photobiomodulation (PBM) improve Alzheimer's disease (AD) pathology. PBM enhances mitochondrial respiratory by photoreceptor cytochrome c oxidase (*CCO*), which promotes the production of Adenosine Triphosphate (ATP); inhibites neuronal apoptosis by regulating mitochondrial energy metabolism; regulates microglial polarization and autophagy, promoting Aβ clearance, reducing neurological damage. Ultimately, improving cognitive impairment in AD. Scheme1 was created by Figdraw

that PBM can regulate microglial polarisation and inhibit neuronal apoptosis, the relationship between PBM-mediated regulation of mitochondrial energy metabolism and these effects has not yet been established. Moreover, the mechanism of action of PBM in neurological injury requires further investigation.

In this study, we used 808 nm PBM to intervene in double transgenic APP/PS1 mice, and the effects of PBM on cognitive function and neurological damage and its mechanism were investigated (Scheme 1). The results demonstrated that PBM inhibited neuronal apoptosis by regulating mitochondrial energy metabolism, attenuating neuroinflammation, regulating microglial polarisation, and promoting Aβ clearance, reducing neurological damage and effectively improving cognitive impairment in AD. This study elucidates the intrinsic mechanism by which PBM ameliorates AD neuronal damage and provides a theoretical basis for the application of non-invasive phototherapy in neurological diseases.

Materials and methods

Animals and treatment

All mice used in this experiment were purchased from Weitong Lihua Laboratory Animal Technology Co., Ltd (Beijing, China). Richard et al. found that 2-month-old 5xFAD mice did not show any neurological changes, except for alterations in anxiety behavior [30]. Cognitive deficits occur at about 5 months of age, and neuronal loss in brain regions with amyloidosis begins at 6 months of age [30]. In APP/PS1 mice, amyloid deposits in brain between 4 to 6 months and cognitive deficit occurs between 6 to 10 months [31, 32]. Therefore, we selected 6-month-old APP/PS1 double transgenic mice and 6-month-old C57BL/6 J mice. Mariscal et al.'s study showed that female mice performed better at recognizing objects with small differences and showed higher emotional excitement responses than male mice [33]. It can be seen that female mice are more conducive to observing indicators of cognitive function changes. In addition, in the selection of sex in mice, we also referred to the study of Tao et al. on phototherapy AD [13]. All experimental mice (females) were acclimatized to the experimental environment by normal feeding for 3 days. The Animal Care and Experimental Program was approved by the Institute of Radiological Medicine, Chinese Academy of Medical Sciences (ethical review no. IRM-DWLL-2023017).

C57BL/6 J mice were designated as the Control (CON) groups ($n=6$). The APP/PS1 mice were randomly divided into two groups: one designated as the AD group and the

other designated as the PBM group ($n=6$ per group). The CON and AD groups were maintained under standard conditions throughout the experiment, with no intervention. The PBM group used a self-constructed LED phototherapy apparatus with an 808 nm wavelength, a light intensity of 20 mW/cm^2, and 10-min irradiation twice daily for 6 weeks. Before phototherapy, the hair at the top of the skull was shaved off in the PBM group to facilitate absorption of NIR radiation.

Behavioral testing

Morris water maze

The Morris water maze (MWM) experiment was conducted in a black circular tank (diameter: 150 cm; height: 60 cm). The water temperature in the tank was maintained at 22 ± 1 °C, and white food was added to facilitate the observation of the swimming trajectories of the mice. The four quadrants of the circular water tank were marked with different patterns to serve as spatial references. An escape platform (10 cm diameter, circular) was placed in the target quadrant at a depth of 1 cm. During the learning phase, the mice were randomly introduced into different quadrants and allowed to search for the hidden platform for 90 s. Following positioning of the platform, the mice were left on it for 30 s to memorise the spatial cues. The platform remained in its original position throughout the experiments. During the test phase, the platform was removed from the tank, and the experimental animal was released from the opposite side of the quadrant where the original platform is located. A camera recorded the time taken for the mouse to reach the original platform, number of times the platform crossed, and proportion of the target quadrant within 90 s.

Open field test

The open-field test (OFT) box (length × width × height: 60 × 60 × 40 cm) was a white, uncovered device with an elevated pole above it to instal the camera. Before the start of the experiment, the mice were left move freely in the experimental box for 5 min to acclimatize to the experimental environment. The mice were then positioned in the experimental box from a central position and their movements were observed for 5 min. Following the completion of each trial, faeces within the experimental box were cleaned and the box disinfected with an alcohol-based solution. The trajectories and behaviours of the mice in the experimental box were recorded for subsequent analysis.

Tissue collection

After the behavioral test was completed, mice were perfused with phosphate-buffered saline (PBS) after anesthesia. The brains were rapidly extracted and divided into two groups as needed for the experiment. One of the groups was fixed in 4% paraformaldehyde (PFA). Another group was freshly frozen on ice. The cortex and hippocampus were isolated from fresh brains, weighed and placed in cryovials for storage at—80 °C. Fixed brains are stored in 4% PFA for 24 h at 4 °C and then transferred to PBS in 30% sucrose solution for 48 h for dehydration. Subsequently, embed in paraffin and stored at −80 °C until used for section observation.

Immunohistochemistry and immunofluorescence

The embedded paraffin blocks were removed and deparaffinised in xylene. For immunohistochemistry experiments, brain slices were heated in citrate buffer for 30 min to perform antigen retrieval. For immunofluorescence experiments, sections were rinsed with PBS. For immunofluorescence experiments, the sections were rinsed with PBS. Then, sections were incubated with a blocking solution (containing PBS, 5% bovine serum albumin, and 0.3% Triton X-100) for 1 h at 25 °C. After the 25 °C incubation, sections were co-incubated with the primary antibody overnight at 4 °C. The primary antibodies used were anti-Aβ (AB201060, ABCAM), anti-Arg-1 (16,001–1-AP, Proteintech Group, Inc.), anti-CD86 (bs-1035R, Bioss), NLRP3 (ET1610-93, HUABIO), and anti-glial fibrillary acidic protein (GFAP) (60,190–1-Ig, Proteintech Group, Inc.). The following antibodies were used: anti-IBA1 antibody (10,904–1-AP, Proteintech Group, Inc.), mouse anti-Cytc (bsm-33193 M, Bioss), and monoclonal anti-HK2 (66,974–1-Ig, Proteintech Group, Inc.). Subsequently, the slices were washed thrice with PBS. Subsequently, the sections were incubated with the corresponding secondary antibodies at 25 °C for 1 h, after which they were washed three times with PBS. In immunohistochemical experiments, the nuclei were re-stained with haematoxylin, dehydrated, and sealed. For the immunofluorescence experiments, the sections were incubated with DAPI for 5 min, after which they were sealed. Among them, TSA-FITC staining solution should be added to the three-staining experiment. Imaging was performed using a confocal microscope.

Nissl and Haematoxylin & eosin staining

The paraffin sections were de-paraffinised in xylene, and Nissl staining was performed using a toluidine blue staining solution (G1434, Solarbio, China). For haematoxylin and eosin (HE) staining, the sections were incubated in haematoxylin solution, washed, and stained with eosin solution with dehydration and transparency. The sections

were then sealed with neutral adhesive and imaged using a confocal microscope.

Enzyme-linked immunosorbent assay (ELISA)

Whole blood was extracted from the retroocular venous plexus of mice and left for 30 min. The mixture was then centrifuged to obtain the supernatant (1200 rpm, 5 min), which was stored at − 80 °C. Subsequently, blood was removed and stored in a cryotube. The mice were anaesthetised, and the brain tissue was rapidly collected, placed in cryotubes, and stored at − 80 °C.

The presence of inflammatory factors and apoptotic proteins was determined using ELISA (Shanghai Tongwei Biotechnology Co,. LTD.). The hippocampus was weighed, then placed the hippocampus in a tissue grinder and pre-chilled PBS was added (pH 7.0—7.2) in a ratio of ice PBS: tissue weight = 9:1 and the tissue was ground thoroughly. Then the homogenate was placed at 4 °C, centrifuged at 10,000 r/min for 20 min, and the supernatant was extracted for later use. Finally, perform an ELISA assay was performed according to the manufacturer's instructions, using a microplate reader to detect the absorbance at 450 nm.

Assay for mitochondrial membrane potential (MMP)

Brain tissues were placed in a tissue grinder, the lysate was added after thorough grinding, and the supernatant was discarded after centrifugation. A total of 0.5 ml of JC-1 staining solution (Beyotime, Shanghai, China) was added to the samples, which were then incubated at 37 °C for 20 min. Subsequently, the samples were centrifuged for 3 min, and the supernatant was discarded. The samples were then resuspended twice in JC-1 and centrifuged for 3 min, and the resulting supernatants were discarded. The samples were then resuspended in a JC-1 stain and analysed by flow cytometry.

Quantitative reverse transcription polymerase chain reaction (RT-PCR)

The brain tissue was ground in a tissue grinder at a low temperature. TRIzol solution (Beyotime, Shanghai, China) was then added, and the cells were lysed for 5 min at 25 °C. Chloroform (200 μL) was added to the tissue suspension, which was allowed to stand for 10 min. Subsequently, centrifugation (12,000 g, 15 min, 4 ℃) was performed to extract the supernatant. The mixture was agitated for 10 min with the addition of 500 μL of isopropanol. The supernatant was discarded, and the RNA precipitate was obtained. The mixture was then washed with 75% ethanol and centrifuged (7500 g, 10 min, 4 ℃). After allowing the precipitate to dry for 10–15 min, it was dissolved in 30 μL of DEPC solution (Solarbio, China) and the RNA concentration was determined by microspectrophotometer. Moreover, cells were cultured in 6-well plates and total RNA was extracted 4 h after the completion of light treatment using the TRIzol method.

The mRNA expression levels were quantified by RT-PCR on an ABI 7900HT Fluorescence Quantitative PCR Instrument using the TB Green® Premix Ex TaqTM kit (Takara, Japan). The expression level of GAPDH/β-actin was used as the reference, and qPCR signals were quantified using the $2^{-\Delta\Delta Ct}$ method. We list the primers used in this study in Table 1.

Western blotting analysis (WB)

The weighed brain tissue was placed in a grinding tube containing lysate and grinding beads, and then the tube was placed in a grinder at − 30 °C for thorough grinding. Milled tissues were lysed on ice for 20 min. The protein concentrations in the sample were quantified with a biquinone acid kit. A corresponding volume of 5 × Protein Gel Electrophoresis Sampling Buffer was added to the protein sample, mixed, and denatured for electrophoretic separation. Subsequently, the membranes were transferred onto polyvinylidene fluoride membranes.

Table 1 Primer sequences used for real-time PCR

Target primer name	Target primer sequences
BCL2F	CTACGAGTGGGATGCTGGAGA
BCL2R	CTCAGGCTGGAAGGAGAAGATG
BaxF	CAAGAAGCTGAGCGAGTGTCT
BaxR	GCAAAGTAGAAGAGGGCAACCA
Caspase3F	CAGGAAGGTGGCAACGGAAT
Caspase3R	TCGTGAGCATGGACACAATACA
Caspase9F	GCCACTGCCTCATCATCAACA
Caspase9R	GCGGAATCGGTGCTCAAGTT
HK2F	GACCAGAGCATCCTCCTCAAGT
HK2R	CGGCGAATGGCTTCCTTCAG
cytcF	GGAGGCAAGCATAAGACTGGA
cytcR	TTGTTCTTGTTGGCATCTGTGT
TSPOF	GGGAGCCTACTTTGTACGTGG
TSPOR	TGAAACCTCCCAGCTCTTTCC
LC3IIF	AGCCTTCTTCCTCCTGGTGAATG
LC3IIR	TGCTGTCCCGAATGTCTCCTG
Beclin1F	CAGGCTGAGGCGGAGAGATTG
Beclin1R	GGAAGGTGGCATTGAAGACATTGG
β-actinF	AGAAGCTGTGCTATGTTGCTCTA
β-actinR	TCAGGCAGCTCATAGCTCTTC
GPADHF	ACAACTTTGGTATCGTGGAAGG
GPADHR	GCCATCACGCCACAGTTTC

Table 2 Primary antibodies used in the WB experiment

Antibody name	Item number	Dilution factor
NLRP3(118 kD)	BOSTER(BA3677)	1:1000
Cytc(16 kD)	BOSTER(A00961-2)	1:1000
Caspase3(35,19,17 kD)	CST(14220S)	1:1000
Caspase9(46 kD)	Proteintech(10,380–1-AP)	1:700
GLUT1(45–55 kD)	Proteintech(21,829–1-AP)	1:4000
PKM2(58 kD)	Proteintech(158,221–1-AP)	1:2000
PGC1(92–100 kD)	Proteintech(66,369–1-1G)	1:1000
CD86(74kd)	BIOSS(bs-1035R)	1:1000
ARG1(35kd)	Proteintech(16,001–1-AP)	1:1000
HK2(102kd)	Proteintech(66,974–1-1 g)	1:10,000
NRF1(70 kD)	Proteintech(66,832–1-1G)	1:20,000
LC3II(15,18 kD)	BOSTER(PA01524)	1:1000
Mouse β-tubulin(55kD)	ZSGB-BIO(TA-10)	1:2000

Then, the membrane was incubated with the primary antibody at 4 °C overnight. The membrane was then washed three times with 1×TBST and incubated with the secondary antibody for 1 h at 25 °C. Finally, the grey scale values were analysed using ImageJ software. The primary antibodies used are listed in Table 2.

Cell culture and treatment

BV2 cells (mouse microglia, CL-0493A) were obtained from Wuhan Procell Biotechnology Co. and maintained in a specialised BV2 medium (Procell, CM-0493A). The cell experiments were conducted in two groups. The experimental groups were designated as follows: CON, PBM; LPS, LPS+PBM; and CON, LPS, LPS+PBM, 3BP. The LPS, LPS+PBM, and 3BP groups were induced by the addition of 2 μg/mL LPS (Solarbio, L8880) (This parameter was determined by our previous study [34]) 24 h after cell inoculation, whereas the remaining groups were treated with DMEM/F12 (Dulbecco's modified Eagles medium)basal medium (Gibco, C11330500BT). Following a 24 h incubation period, the medium of each experimental group was changed to BV2 cell-specific medium, except for that of the 3BP group, which was replaced with a 33.3 μM 3BP solution (Selleck, S5426).

Through the study of the cell proliferative activity of 808 nm PBM at different energy densities on fibroblastsand endothelial cells, we found that PBM had the best promoting effect on cells at an energy density of 3 J/cm^2. In addition, Rafaella Carvalho et al. irradiated hydrogen peroxide (H_2O_2)-induced SH-SY5Y cells (human neuroblastoma) with 660 nm LEDs to compare the neuroprotective effects of LED irradiation at different energy densities on the cells [35]. The results showed that the energy density of 3 J/cm^2 was the lowest one that obtained better statistical increase in mithocondrial activity ($p<0.0001$) [35]. Therefore, in this experiment, we used a low-intensity semiconductor laser with a wavelength of 808 nm was used to irradiate the PBM group at a power of 20 mW/cm^2, with each subject undergoing two daily irradiations at a dose of 3 J/cm^2. The remaining groups were not irradiated and were maintained under identical conditions.

Immunofluorescent staining

Immunofluorescence assay of microglial phenotype

The microglia were plated in 24-well plates for cell culture and light treatment. Following completion of the light treatment, the following operations were performed 4 h later. Cells were fixed in 4% paraformaldehyde and incubated with Triton X-100 and 5% goat serum. Subsequently, the cells were incubated overnight at 4 °C with the primary antibody followed by a 1-h incubation at 25 °C with the secondary antibody the following day. The primary antibodies used were anti-CD86 (Solarbio, K000343P) and anti-ARG1 (Solarbio, K009684P), whereas the fluorescent secondary antibodies were labelled as follows: goat anti-rabbit IgG/RBITC (Solarbio, SR134). The plates were incubated with DAPI for 5 min to protect them from light, after which a drop of an anti-fluorescence quencher was added to seal the plates. The images were then captured.

Immunofluorescence assay of microglia phagocytosis

The slides of cells were sterilized and placed in 24-well plates, and 1×10^5 microglia were added to each well and cultured for 24 h. Then, 1 mL of 2 μg/mL LPS was added for 24 h inflammation modeling, and phototherapy was performed after the modeling was completed. 4 h after the end of photostimulation, 500 nM FAM-Aβ_{1-42} (AnaSpec, AS-23526–01) was added to each well and incubated at 37 °C for 30 min in the dark. Subsequently, the wells were washed twice with PBS, and 500 μL of a solution of LysoTracker Red (Beyotime, C1046) was added and incubated for 30 min at 37 °C in the dark. After washing with PBS, images were acquired.

Although oligomeric Aβ is more physiologically relevant, monomeric Aβ was used in this experiment. There are two main reasons for this. First of all, oligomer Aβ has a higher tendency to aggregate and is easy to further aggregate into fibrous or plaque-like, and its aggregation state is greatly affected by various factors such as temperature, pH value, ionic strength, etc., and it is difficult to maintain a stable oligomeric state during the experiment. Compared with oligomeric Aβ, monomeric Aβ is more structurally stable under specific conditions, which is easier to store and maintain a relatively uniform state in the experimental system, which is conducive to the reproducibility and

accuracy of experimental results. In addition, due to its aggregation characteristics, oligomeric Aβ is prone to precipitation or uneven distribution during dissolution and dispersion, which brings inconvenience to experimental operations. The solubility of monomeric Aβ in solution is usually better, making it easier to prepare solutions of different concentrations for experiments. In addition, literature research has found that some of the studies used experiments with Aβ monomers [36–38].

ROS level assay

Laser scanning confocal microscope: The cells were cultured in 6-well plates, and ROS levels were detected 4 h after the end of photostimulation. A total of 500 μL DCFH-DA solution (Beyotime, S0033S) was added to each well and incubated at 37 °C in the dark for 20 min. Subsequently, the supernatant was removed by washing with a DMEM/F12 basal medium, after which the images were captured. Images were acquired using a laser scanning confocal microscope and fluorescence intensity was analyzed using ImageJ software.

Flow cytometry detection: Cells were inoculated into 6-well plates and cultured according to an established cell culture method. At 4 h post-light treatment, the cells were washed twice with PBS and 500 nM FAM-$A\beta_{1-42}$ was added. The cells were incubated for 1 h at 37 °C in the dark, washed slowly, collected, centrifuged, and resuspended in PBS. Finally, the number of FITC particles was determined using flow cytometry.

Detection of cellular inflammatory factors and cellular ATP levels

The cells were cultured in 6-well plates, and 4 h after the completion of the light treatment, the supernatants were collected and centrifuged before being extracted as assay samples. The levels of inflammatory factors were quantified using ELISA kits, as previously described, with absorbance measured at 450 nm. The cells in 6-well plates were washed with PBS, lysed, and centrifuged to extract the supernatant. ATP levels were quantified using ATP assay kits (Beyotime, S0026) with samples assayed using multifunctional enzyme markers.

Statistical analysis

The statistical analysis of data and figure production was conducted using GraphPad Prism 8.0 software. Student's t test was employed for comparing two groups, while One-way analysis of variance (ANOVA) was used for comparisons among multiple groups. Data were presented as the mean ± standard deviation (SD). The threshold for statistical significance was set at $p < 0.05$, below which the results were considered statistically significant. For image quantification, ImageJ was used.

Results

PBM ameliorates cognitive deficits in APP/PS1 mice

Figure 1A shows the experimental flow of our animal experiments. The MWM test, a behavioural experiment designed to assess learning and memory in rodents, was conducted after a 6-week phototherapy intervention. The trajectory plots of MWM demonstrated that AD mice are more inclined to move against the wall around the periphery of the maze (Fig. 1B). Furthermore, through the comparison between the AD group and the CON group, it can be seen that the spatial learning and memory ability of the AD group decreased significantly, which was manifested by the prolongation of the latency period, the reduction of the number of crossing the platform, and the shortening of the residence time in the target quadrant (Fig. 1C). In contrast, the PBM group exhibited shorter latency, crossed the platform more frequently, and remained longer in the target quadrant compared to the AD group (Fig. 1C). These findings indicate that PBM may be an effective intervention to improve memory loss in AD mice.

The OFT is one of the most frequently used tests for the detection of anxiety-like behaviours in animals. The purpose of this experiment was to investigate whether AD induces anxiety-like behavior in mice and whether PBM has an ameliorating effect on this effect. As illustrated in the trajectory diagram, the AD group showed a pronounced performance of anxiety-like behaviours compared with the CON group, as evidenced by a reduction in the number of shuttles in the central region and a tendency to stand still. Following phototherapy, the number of traversals in the central region of AD mice increased, and spontaneous activity increased (Fig. 1D). Furthermore, the AD group exhibited lower horizontal scores and shorter dwell times in the central area than did the CON group, indicating a reduction in exploratory behaviour and an increase in tension and anxiety levels. Conversely, the PBM group exhibited elevated horizontal scores and dwell times in the central zone following phototherapy. However, the observed differences were not statistically significant (Fig. 1E). These findings indicated that PBM has a beneficial effect on anxiety levels in mice. In conclusion, behavioral experiments have shown that PBM can improve cognitive dysfunction in AD mice.

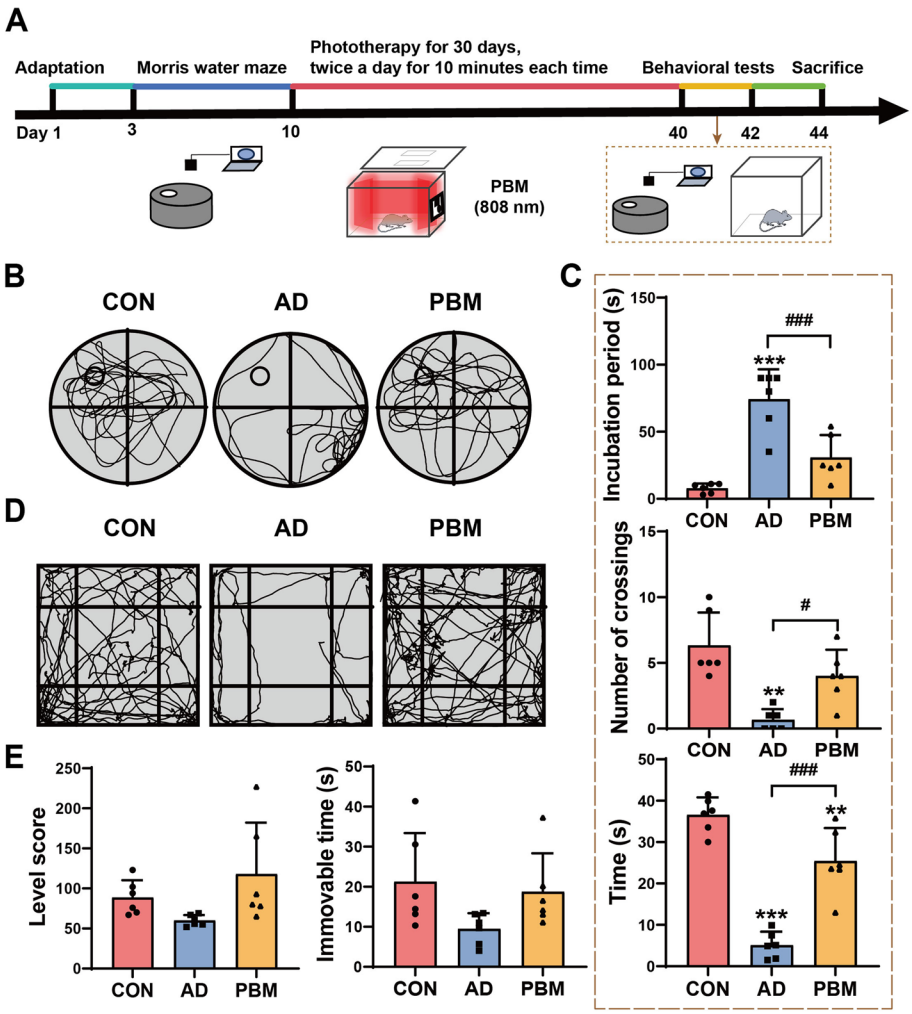

Fig. 1 Photobiomodulation (PBM) ameliorates cognitive deficits in AD mice. **A** Experimental timeline showing 808 nm light treatment and behavioural tests. **B** Representative swimming track of mice in Morris water maze (MWM) test. **C** Bar graphs of latency to find the escape platform, platform crossing number, and time in target quadrant in the test session of MWM. **D** Representative movement tracks in open field test (OFT). **E** Bar graphs of level score and time in centre of the OFT. Experimental data are presented as the mean ± standard deviation, $n = 6$ mice per group. Compared with the CON group, $^{**}p < 0.01$, $^{***}p < 0.001$; Compared with the AD group, $\#p < 0.05$, $\#\#\#p < 0.001$

PBM improves neuronal damage and inhibits astrocyte reactivity in mice with AD

The presence of lesions in the brain can lead to astrocytosis and the occurrence of a reactive inflammatory state [39, 40]. This study aimed to elucidate the effects of PBM intervention on Aβ deposition and astrocytes reactivity. Immunofluorescence double-staining experiments were performed for GFAP, an astrocyte marker, and Aβ. As illustrated in the fluorescence graphs, astrocytes are clustered near Aβ (Fig. 2A). Furthermore, besides the green fluorescence intensity of GFAP, the red fluorescence intensity representing Aβ in the AD group was also substantially higher than that of the CON group (Fig. 2B). This indicated that Aβ may induce astrocyte activation. A comparison of the PBM and AD groups revealed that red fluorescence, indicative of Aβ deposition, was reduced in the PBM group. Moreover, the green fluorescence of GFAP was substantially diminished, and the number of reactive astrocytes that aggregated near Aβ was reduced. These findings suggest that PBM can reduce Aβ deposition and inhibit astrocyte reactivity in mice with AD.

The state of neurons in mouse brain tissue was observed using Nissl and HE staining. As illustrated in Fig. 2B, neurons in the CA3 region of the hippocampus in

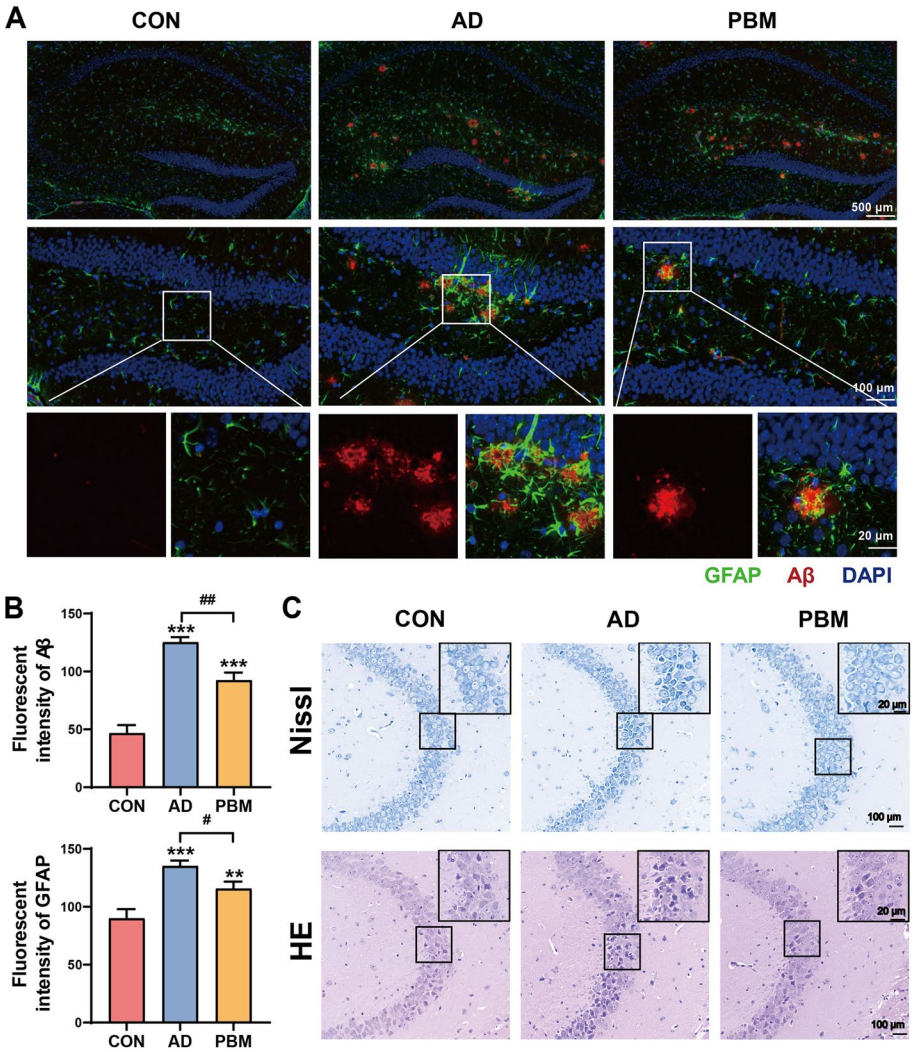

Fig. 2 PBM improves neuronal damage and inhibits astrocyte activation in AD mice. **A** Immunofluorescence double staining of mouse brains using anti-Aβ antibody (red) and anti-GFAP antibody (green) (scale bars 500 μm, 100 μm, and 20 μm, respectively). **B** Mean fluorescence intensity of Aβ and GFAP. **C** Nissl and HE staining plots of the hippocampal CA3 region in mice (scale bars 100 μm and 20 μm, respectively). Experimental data are presented as the mean ± standard deviation. Compared with the CON group, $^{**}p < 0.01$, $^{***}p < 0.001$; Compared with the AD group, $\#p < 0.05$, $\#\#p < 0.01$

the CON group exhibited greater morphological regularity and a neat arrangement. However, compared to that in the CON group, the number of positive neurons in the AD group was substantially reduced. Furthermore, there was nuclear coagulation, and Nissl bodies were ruptured, and the staining intensity increased, indicating that the neurons in the AD group were damaged. The neurons in the PBM group were more neatly arranged, the number of positive neurons was substantially increased compared to that in the AD group, and the nuclei were less consolidated. However, a few ruptured Nissl bodies remained (Fig. 2C). These findings indicate that PBM exerts a protective effect against neuronal damage in mice with AD.

The influences of PBM in microglial polarization and neuroinflammatory levels in mice with AD

The microglial activation phenotype is closely associated with neurodegenerative diseases, and its activation is substantially correlated with accelerated cognitive decline. Here we aimed to elucidate microglial polarisation in the brains of AD mice (Fig. 3A, B). Immunofluorescence staining revealed higher levels of the M1 microglia marker CD86 and lower levels of the M2 microglia marker Arg-1 in the AD group compared with the CON group. After 6 weeks of PBM treatment, CD86 was significantly decreased and Arg-1 was significantly increased in brain sections of AD mice. A

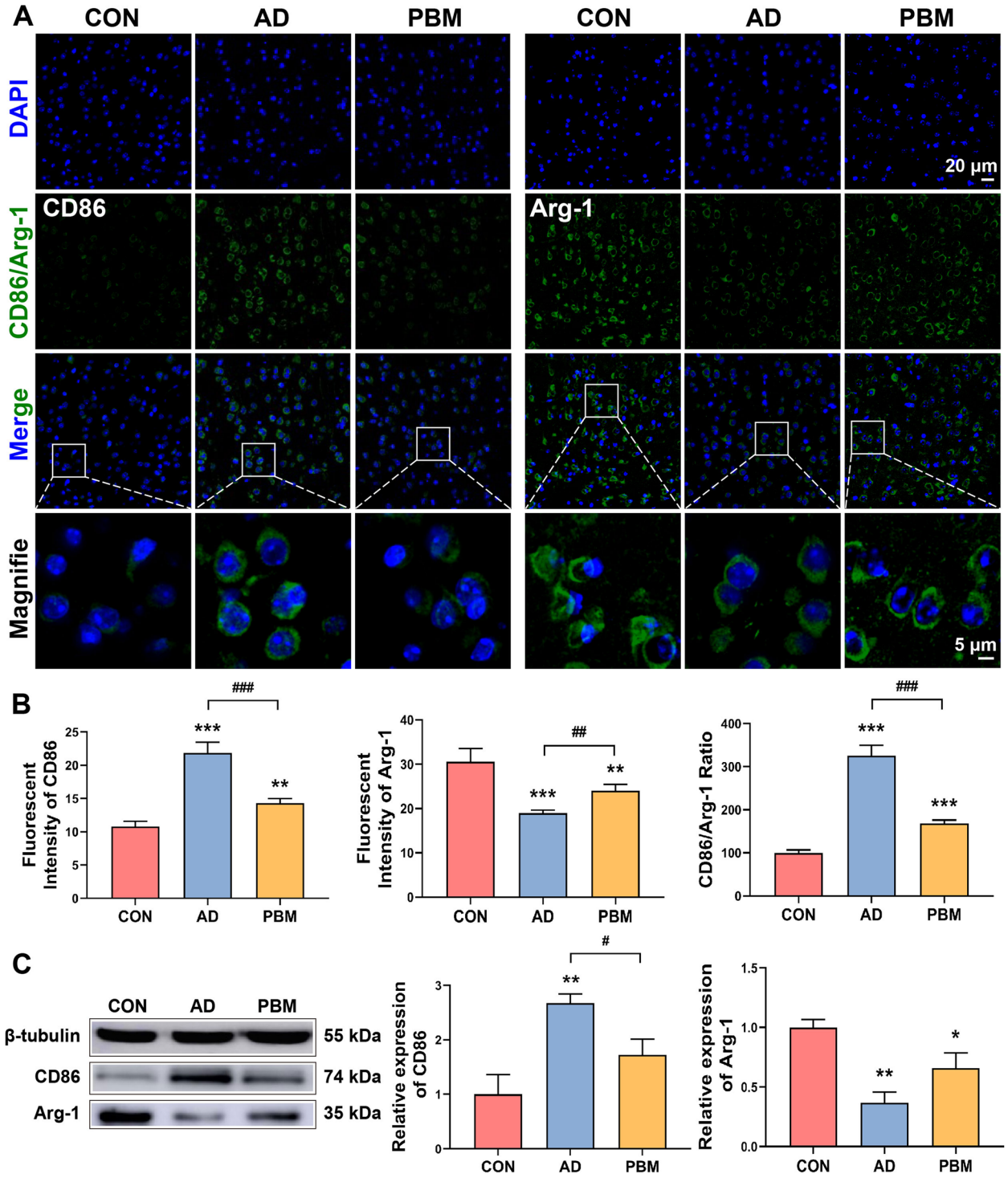

Fig. 3 Effects of PBM on the phenotype of microglia in mice with AD. **A** Representative images of anti-CD86 and anti-Arg-1 immunolabelled microglia in the mouse cortex. Scale bar: 20 μm. A magnified images show typical microglia expressing CD86/Arg-1. Scale bar: 5 μm. **B** Quantitative analysis of the fluorescence intensity and relative ratio of CD86 and Arg-1 in mouse microglia. **C** Exemplary protein immunoblotting and quantification of CD86 and Arg-1 in mouse brain tissue. Experimental data are presented as the mean ± standard deviation. Compared with the CON group, *$p < 0.05$, **$p < 0.01$, ***$p < 0.001$; Compared with the AD group, #$p < 0.05$, ##$p < 0.01$, ###$p < 0.001$

comparison of M1 and M2 type markers revealed that the PBM group exhibited a substantially reduced ratio compared to the AD group, indicating that microglial M2 phenotype polarisation was dominant. Moreover, the analysis of polarisation markers demonstrated that PBM treatment was able to reduce CD86 protein expression in mice with AD (Fig. 3C). The above findings indicate that PBM reduces M1 polarisation and promotes microglial polarisation towards M2.

Microglia can recognise and phagocytose abnormal factors, such as Aβ or Tau, to maintain homeostasis within the brain. IBA1 (microglial marker) and Aβ were labeled by immunofluorescence to observe the changes of PBM on microglial phagocytosis (Fig. 4A). Aβ plaques aggregation were observed in the hippocampus and cortex of AD group mice, and microglia are recruited around the plaques. Manders' Colocalization Coefficients (MCC) provides a visual measure of colocalization and is able to show the overlap between fluorescences. We performed a colocalization analysis of microglia and Aβ using ImageJ, MCC scores were then used to assess the ability of microglia to clear plaques. MCC scores in both hippocampus and cortex in the PBM group were higher than those of the AD group (Fig. 4B). The results show that following PBM intervention, microglia exhibited a greater degree of recruitment around Aβ plaques and phagocytosis, thereby reducing the deposition of the Aβ. ELISA demonstrated that AD mice had lower levels of the anti-inflammatory factors interleukin (IL)−4 and IL-10, while higher levels of pro-inflammatory factors tumour necrosis factor-α (TNF-α), interleukin IL-1β, and IL-6 compared with CON mice (Fig. 4C, D). The level of inflammatory factors in AD mice in the PBM group was significantly reversed, indicating that PBM regulated the secretion of inflammatory factors.

AD mice have a high number of Aβ plaques within their brains, microglia exhibited continuous activation, which resulted in the release of inflammatory mediators. The Nod-like receptor protein 3 (NLRP3) inflammasome has been considered a key contributor to neuroinflammation; it is able to activate caspase-1 to produce inflammatory factors [41]. WB analysis revealed that NLRP3 protein strip width in the AD group was higher than that in the CON group (Fig. 5A). The PBM group exhibited a notable reversal in the level of inflammatory factors in AD mice, indicating that PBM regulates the secretion of inflammatory factors. However, the WB for NLRP3 show overall levels in the whole brain. As it has been shown that both astrocytes and microglia are involved in neuroinflammation and have a crosstalk in AD mouse models [42]. To more accurately analyze the effect of PBM on NLRP3 expression in different cell types, we performed co-fluorescence staining using NLRP3, GFAP and IBA1 (Fig. 5B). From the figure, we can observe that changes in NLRP3 expression in AD mice after PBM intervention occurred in both microglia and astrocytes. And the same as the WB experiment results, NLRP3 expression decreased after PBM intervention. Quantitative analysis of MCC showed that the co-localization of NLRP3 and two types of cells in AD mice after PBM treatment increased (Fig. 5C, D).

These findings indicate that PBM promotes the M2 phenotype of microglia and enhances Aβ phagocytosis, reducing neuroinflammation and alleviating AD symptoms.

PBM inhibits neuronal apoptosis in mice with AD

Apoptosis is the principal manifestation of neuronal damage. In this study, we initially employed flow cytometry to detect alterations in the MMP, as indicated by JC-1, a classical feature of apoptosis. The Q4-2 region represents a normal neuron that exhibits a larger membrane potential and red fluorescence. In contrast, the Q4-4 region represents an apoptotic neuron that exhibits reduced membrane potential and green fluorescence. Compared with the AD group, the percentage of normal neurons in the PBM group increased, while the percentage of apoptotic neurons was significantly reduced (Fig. 6A, B). The results suggest that PBM may be a potentially avenue to ameliorate the reduction of MMP in AD patients.

To study the influence of PBM on apoptosis-related proteins in AD neurons, we detected the expression of Cytc Bax, Bcl-2, Caspase3, and Caspase9. Cytc expression was substantially higher in the AD group than in the CON group. On the contrary, immunohistochemical experiments confirmed that the expression of Cytc in the PBM group was significantly lower than that in the AD group (Fig. 6C, D). Furthermore, the results of ELISA

(See figure on next page.)

Fig. 4 PBM reduced neuroinflammation in mice with AD. **A** Representative immunofluorescence images of anti-Aβ (red) and anti-IBA1 (green) antibodies in the mouse hippocampus and cortex. Scale bar: 100 μm. A magnified images show the location of typical Aβ in microglia. Scale bar: 20 μm. **B** Manders' Colocalization Coefficients (MCC) scores between microglia (Ch1) and Aβ (Ch2) (tM1, above the auto-threshold of Ch2) in the hippocampus and Cortex. **C** The expression levels of anti-inflammatory cytokines IL-4 and IL-10 in brain tissue of mice. **D** The expression levels of pro-inflammatory cytokines TNF-α, IL-1β and IL-6 in mouse brain tissue. Experimental data are presented as the mean ± standard deviation. Compared with the CON group, *$p < 0.05$, **$p < 0.01$, ***$p < 0.001$; Compared with the AD group, ##$p < 0.01$, ###$p < 0.001$

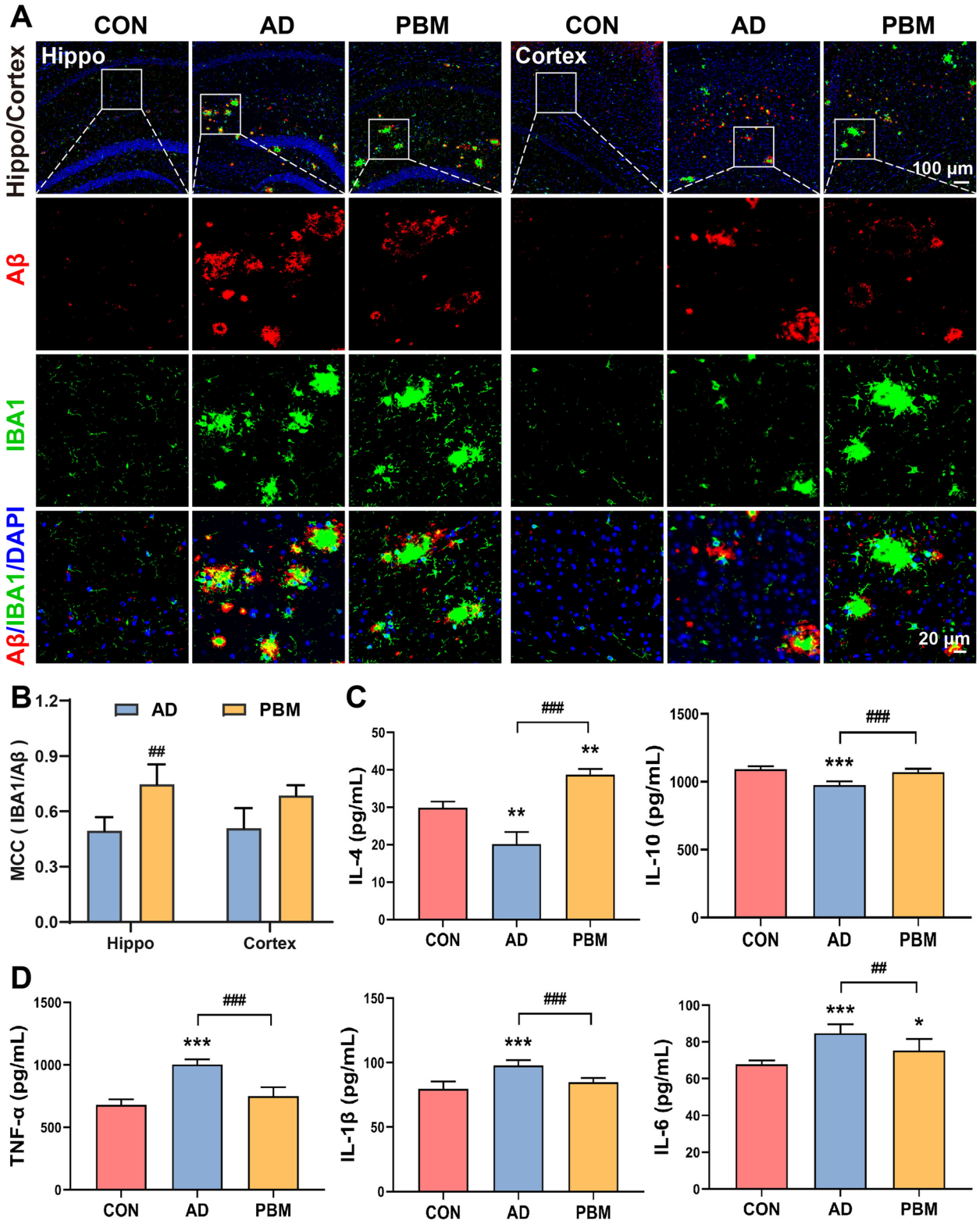

Fig. 4 (See legend on previous page.)

experiments showed that compared with the CON group, the levels of Bax, Caspase3 and Caspase9 in the AD group were substantially elevated, while the level of Bcl-2 was substantially reduced (Supplementary Fig. 1). Conversely, the levels of the pro-apoptotic factor in the brain tissues of mice in the PBM group were substantially reduced, whereas the level of the anti-apoptotic factor was substantially increased compared with those in the AD group. RT-PCR and WB experiments corroborated the above results (Fig. 6E, F). These findings collectively demonstrate that PBM exerts neuroprotective effects in AD mice by inhibiting neuronal cell apoptosis.

PBM ameliorates abnormal mitochondrial autophagy and promotes mitochondrial energy metabolism in mice with AD

Mitophagy is an important self-degradation process in cells, which plays a key role in maintaining the stability of the intracellular environment and regulating energy metabolism. To investigate the effects of PBM on mitochondrial energy metabolism, we examined its effects on autophagy protein levels. The changes of autophagy-related proteins (LC3II and Beclin1) was quantified using RT-PCR and WB analyses. The expression levels of LC3II and Beclin1 were substantially higher in the AD group than in the CON group. The levels of both proteins were substantially reduced after PBM intervention (Fig. 7A, B). The above experiments suggest that PBM is a useful intervention for mitigating the aberrant mitochondrial autophagy in AD.

OXPHOS and glycolysis are the two principal forms of mitochondrial energy metabolism. Subsequently, we examined OXPHOS-related proteins (peroxisome proliferator-activated receptor-γ coactivator-1α (PGC-1α) and nuclear respiratory factor (NRF-1)) and glycolysis-related proteins (glucose transporter protein (GLUT)1, PKM2, hexokinase (HK)2, and TSPO) in the samples. The levels of PGC-1α and NRF1 in the AD group were significantly lower than those in the CON group. PGC-1α and NRF-1 expression levels were elevated in the PBM group (Fig. 7B). Immunohistochemical results demonstrated that the number of brown plaques (HK2) were greater in the brains of AD mice, whereas brown plaques were substantially reduced after PBM intervention (Fig. 7C). Furthermore, the relative protein expression of GLUT1, PKM2, and HK2 in the AD group were substantially increased, and the mRNA expressions of TSPO and HK2 were also substantially higher than those in the CON group. Conversely, the levels of GLUT1, PKM2, and HK2 in AD mice were substantially decreased after PBM intervention (Fig. 7A, D, E).

These findings demonstrate that PBM promotes oxidative phosphorylation, inhibits glycolysis, and restores mitochondrial energy metabolism in mice with AD.

PBM regulates phenotype and improves neuroinflammation in BV2 microglia

Subsequently, BV2 microglia were used to study the influences of PBM treatment on microglia. Following LPS treatment, immunofluorescence staining demonstrated that PBM treatment substantially elevated Arg-1 expression and reduced CD86 expression compared to those in the LPS group (Fig. 8A, B). Furthermore, the ratio of CD86 to Arg-1 in microglia was analysed (Fig. 8C). The ratio was significantly higher in the LPS group. The LPS + PBM group, however, exhibited a significant decrease in the ratio compared to the LPS group. These findings indicate that PBM influences microglial polarisation, promoting a shift towards the M2 phenotype.

Microglia are responsible for maintaining the homeostasis of the CNS by engulfing abnormal substances and forming phagolysosomes with lysosomes for clearance. The capacity of microglia to phagocytose was evaluated using FAM-Aβ_{1-42} (Fig. 9A). In the absence of external stimuli, microglia are responsible for monitoring environmental changes, engulfing pathogens, and clearing them from surrounding areas. The fluorescence intensities of both LysoTracker and FAM-Aβ_{1-42} were lower than those in the CON group after LPS intervention. Both lysosomal and microglial phagocytosis of Aβ was substantially increased in the LPS + PBM group compared to that in the LPS group. Analysis of the fluorescence intensity of Aβ phagocytosis by microglia demonstrated that PBM promoted microglial phagocytic function (Fig. 9B).

LPS induces microglia to secrete pro-inflammatory factors. We measured the level of inflammation in the cell culture supernatant, and the experimental results showed that the levels of pro-inflammatory factors was substantially elevated in the LPS group, whereasthe relative

(See figure on next page.)

Fig. 5 Effect of PBM on NLRP3 inflammasome in mice with AD. **A** Exemplary WB and quantification of NLRP3 in mouse brain tissue. **B** Representative immunofluorescence images of NLRP3 (red), anti-GFAP (orange) and anti-IBA1 (green) antibodies in the mouse hippocampus and cortex (scale bars 100 μm and 20 μm, respectively). **C** MCC scores between astrocyte (Ch1) and NLRP3 (Ch2) (tM1, above the auto-threshold of Ch2). **D** MCC scores between microglia (Ch1) and NLRP3 (Ch2) (tM1, above the auto-threshold of Ch2). Experimental data are presented as the mean ± standard deviation. Compared with the CON group, *$p < 0.05$, **$p < 0.01$, ***$p < 0.001$; Compared with the AD group, ###$p < 0.001$

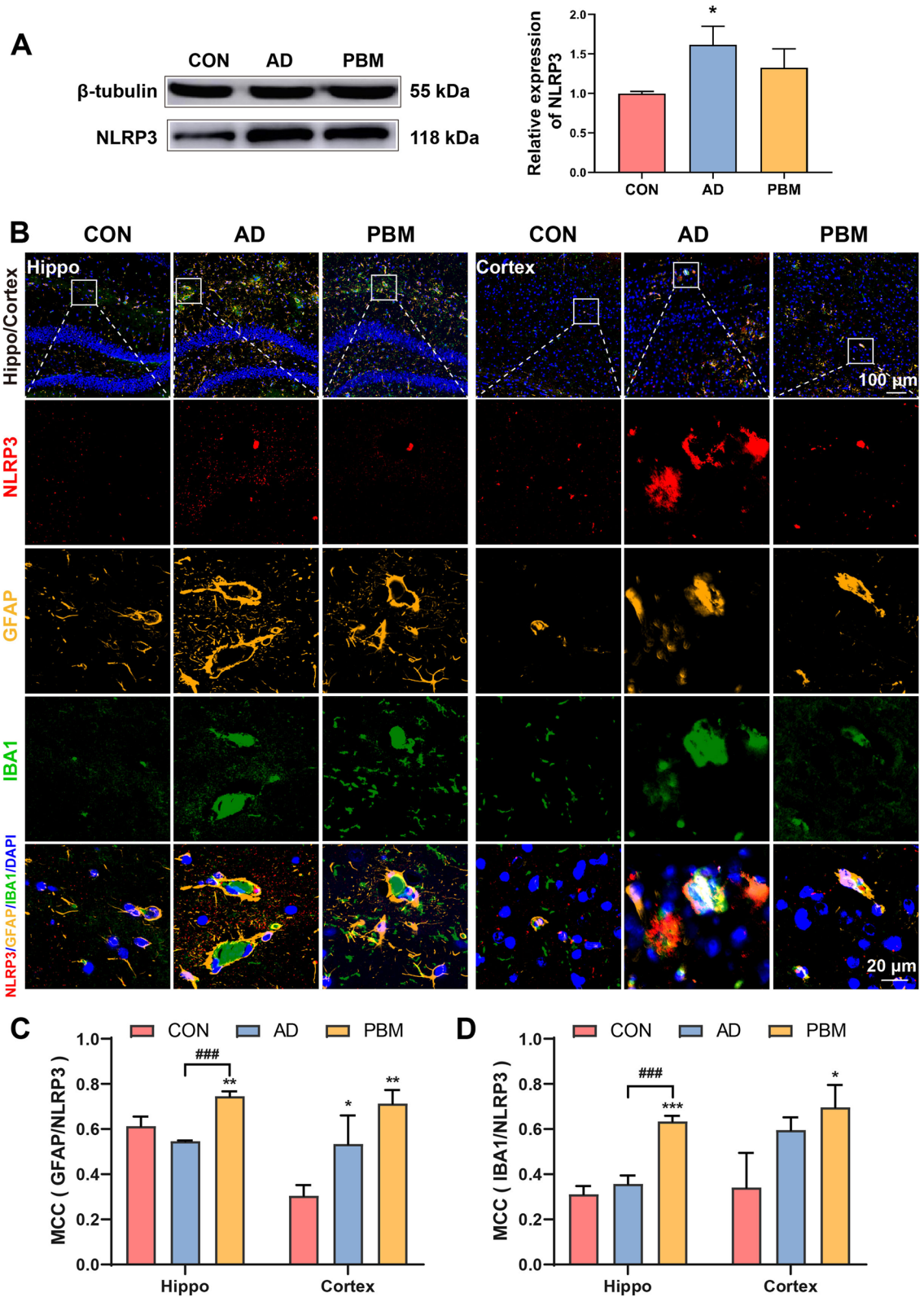

Fig. 5 (See legend on previous page.)

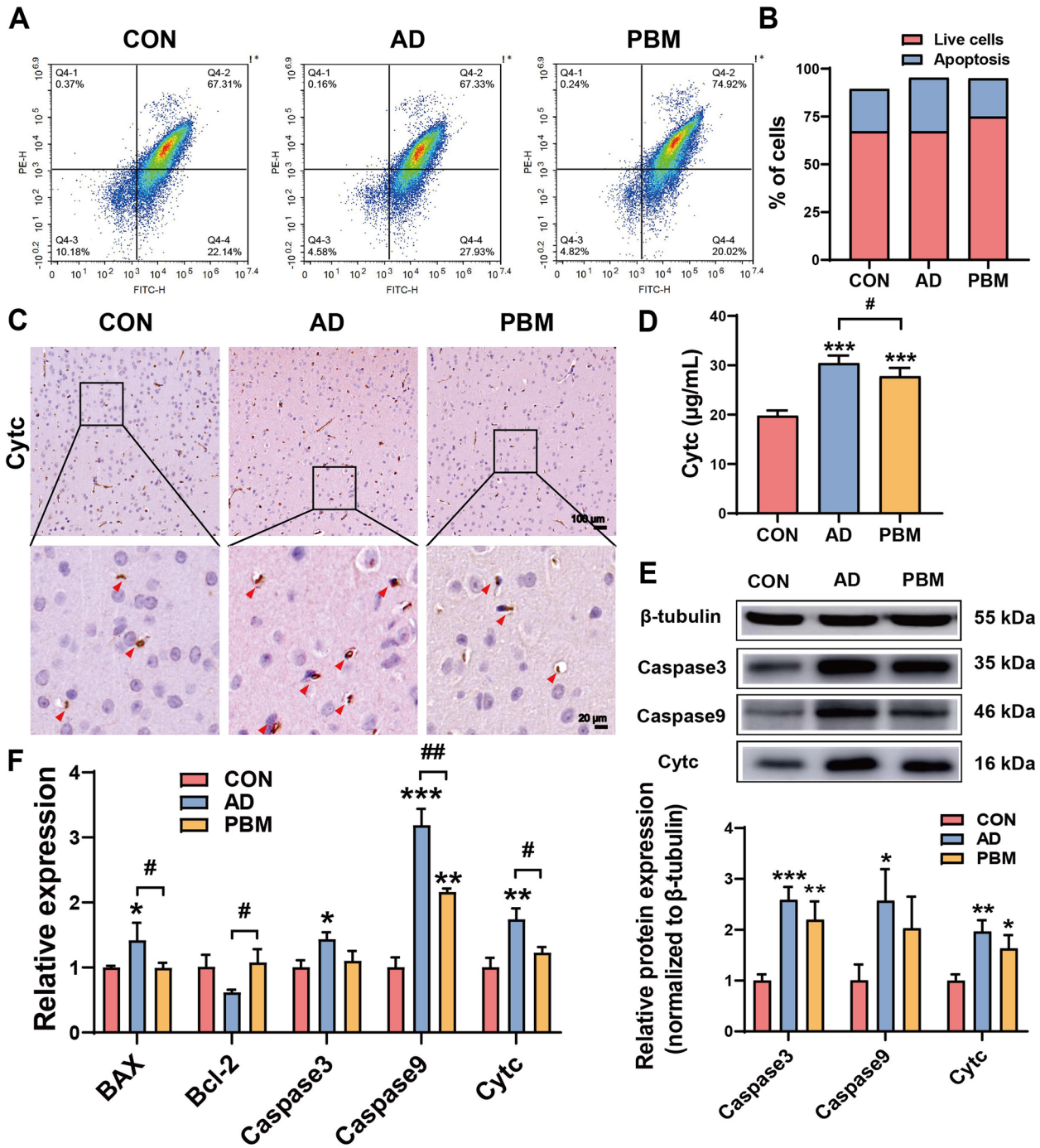

Fig. 6 PBM inhibits neuronal apoptosis in mice with AD. **A-B** Analysis of JC-1 flow cytometry results in the mouse brain tissue. **C** Immunohistochemical staining of mouse brains using an anti-Cytc antibody (scale bars 100 μm and 20 μm, respectively) with arrows indicating Cytc. **D** ELISA was used to detect Cytc in mouse brain tissue. **E** WB was used to detect Caspase3, Caspase9, and Cytc in the mouse brain tissue. **F** RT-PCR was used to detect Bcl-2, Bax, Caspase3, Caspase9, and Cytc in mouse brains. Experimental data are presented as the mean ± standard deviation. Compared with the CON group, *$p < 0.05$, **$p < 0.01$, ***$p < 0.001$; Compared with the AD group, #$p < 0.05$, ##$p < 0.01$, ###$p < 0.001$

levels of anti-inflammatory factors were substantially reduced. The results of the animal experiments with PBM treatment were similarly confirmed in the LPS + PBM group, indicating that it reduced the LPS-induced upregulation of TNF-α and IL-1β expression, while promoting the level of IL-4 (Fig. 9C, D). These findings indicate

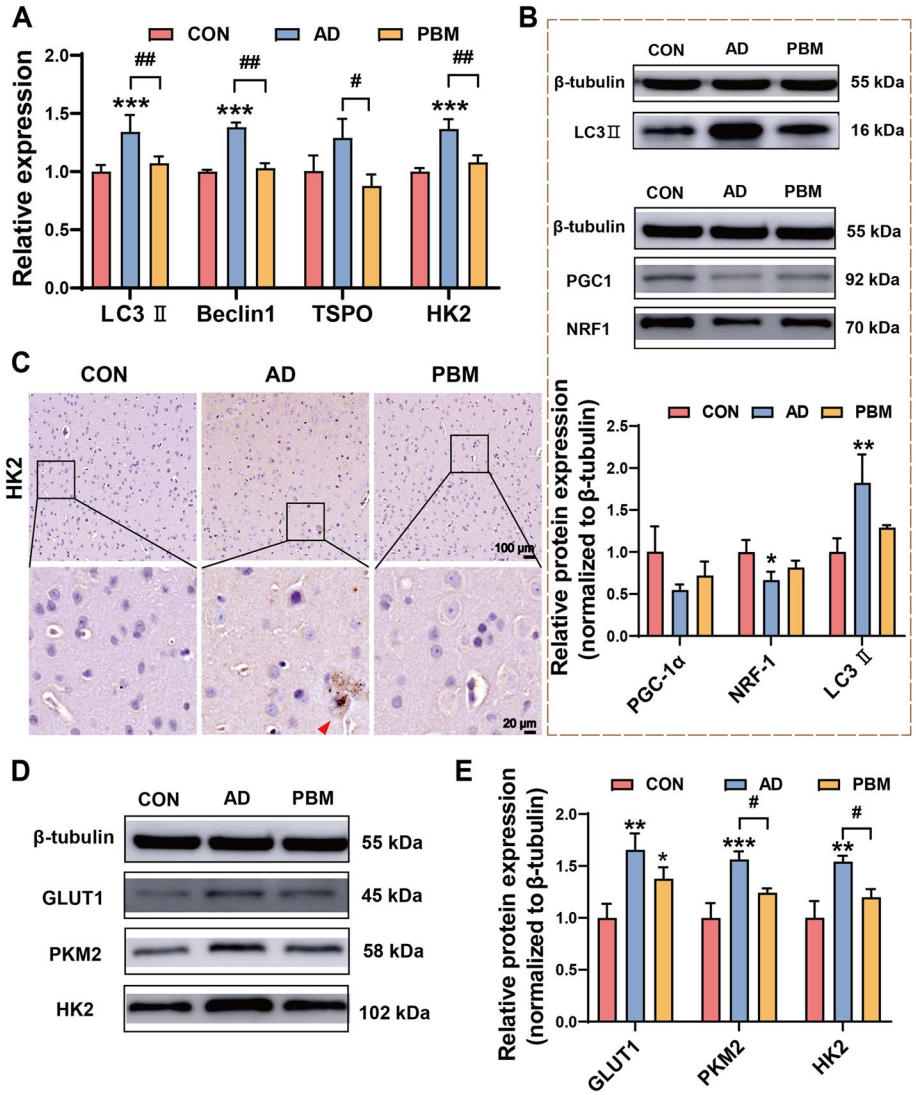

Fig. 7 PBM alleviates abnormal mitochondrial autophagy and promotes mitochondrial energy metabolism in mice with AD. **A** RT-PCR was used to detect autophagy-related protein (Beclin1, LC3II.) and glycolysis-related proteins (TSPO and HK2) in mouse brain tissues. **B** WB was used to detect the autophagy protein LC3II, and the oxidative phosphorylation-related proteins PGC-1α and NRF-1. **C** Immunohistochemical staining of mouse brains using an anti-HK2 antibody (scale bars 100 μm and 20 μm, respectively) with brown plaques of HK2. **D**, **E** WB was used to detect the glycolysis-related proteins GLUT1, PKM2, and HK2. Experimental data are presented as the mean ± standard deviation. Compared with the CON group, *$p < 0.05$, **$p < 0.01$, ***$p < 0.001$; Compared with the AD group, #$p < 0.05$, ##$p < 0.01$

that PBM can regulate the expression level of inflammatory cytokines, thereby inhibiting neuroinflammation. The data presented here demonstrate that PBM regulates microglial activation, inflammation, and phagocytosis.

PBM regulates mitochondrial energy metabolism and phagocytosis in BV2 microglia

In vivo results demonstrated that PBM exerted a significant influence on mitochondrial energy metabolism. Microglia require considerable ATP produced by mitochondria for phagocytosis. Following LPS treatment, BV2 microglia exhibited elevated ROS and substantially reduced ATP levels (Fig. 10A, B). PBM treatment substantially reduced ROS levels and increased ATP production, indicating that PBM may be a useful means for ameliorating disruption of mitochondrial energy metabolism in microglia.

Disorders in mitochondrial energy metabolism can lead to an increase in glycolysis at the expense of OXPHOS, resulting in energy deficits. The results demonstrated that the mRNA levels of glycolysis-related genes HK2 and TSPO were substantially elevated in the LPS group.

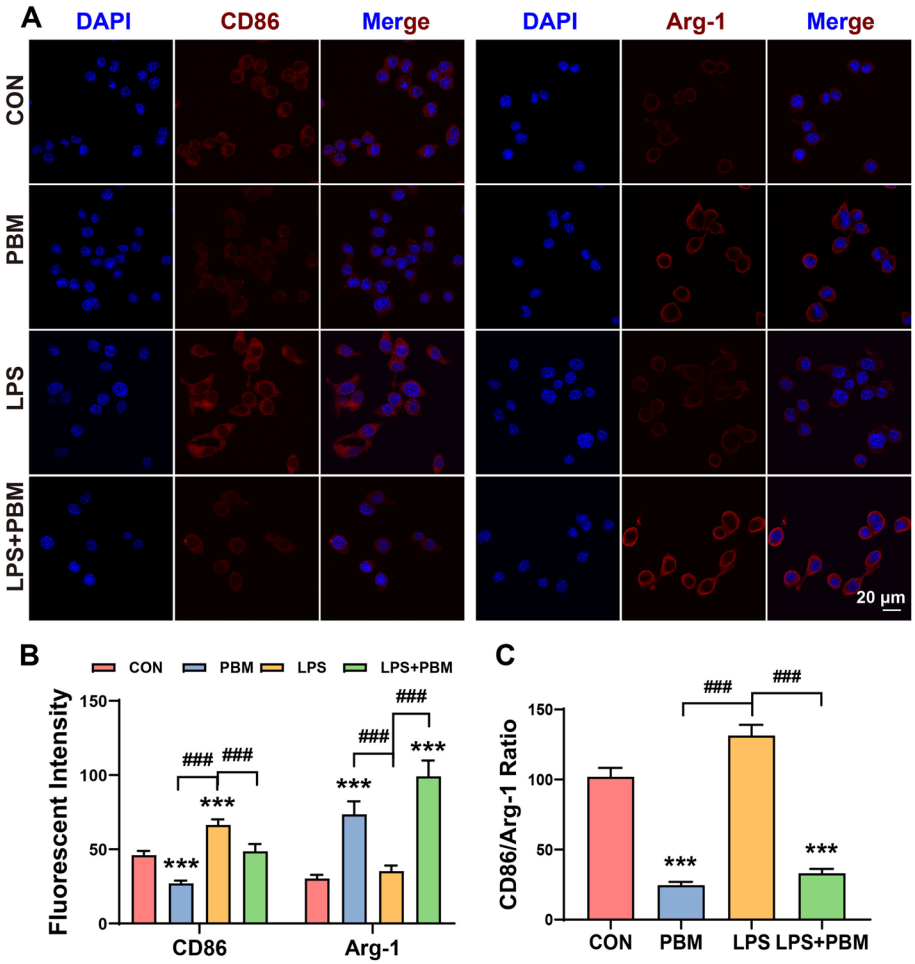

Fig. 8 PBM treatment regulates microglial phenotype. **A** Representative immunofluorescence images of the M1 marker CD86 and M2 marker Arg-1 in microglia cultured in vitro. Scale bar: 20 μm. $n = 4$. **B-C** Quantitative analysis of the fluorescence intensity and relative ratio of CD86 to Arg-1. Compared with the CON group, ***$p < 0.001$; Compared with the LPS group, ###$p < 0.001$

Moreover, the LPS + PBM group shown a pronounced reduction in the elevated HK2 expression observed in the LPS group (Fig. 10C). Our findings indicate that PBM can regulate microglial energy metabolism by reducing the increase in mitochondrial glycolysis.

We aimed to ascertain whether inhibition of HK2 modulates mitochondrial function in microglia. The effects of the HK2 inhibitor, 3BP, on microglia were evaluated. Immunofluorescence assays demonstrated that both HK2 inhibition and PBM treatment reduced ROS levels in inflammatory cells (Fig. 10D). The previous experimental results showed that PBM can modulate inflammation. Therefore, this study explored whether the inhibition of HK2 could have a similar effect. Both PBM intervention and 3BP action significantly altered the expression levels of LPS-induced inflammatory factors (Fig. 10E), suggesting that inhibition of HK2 could inhibit the inflammatory response induced by activated microglia.

(See figure on next page.)

Fig. 9 PBM regulates microglial phagocytosis and reduces inflammation. **A** Representative immunofluorescence images of the lysosomal probes LysoTracker (red) and $A\beta_{1-42}$ (green) in cultured microglia in vitro. Scale bar: 50 μm. A magnified images show typical microglia with lysosomes that engulf Aβ. Scale bar: 10 μm. **B** Relative ratio of FAM-$A\beta_{1-42}$ to LysoTracker in microglia. **C**, **D** Expression levels of anti-inflammatory cytokine IL-4 and the pro-inflammatory cytokines TNF-α, IL-1β in the culture supernatant of microglia in vitro. Experimental data are presented as the mean ± standard deviation. Compared with the CON group, **$p < 0.01$, ***$p < 0.001$; Compared with the LPS group, #$p < 0.05$, ##$p < 0.01$, ###$p < 0.001$

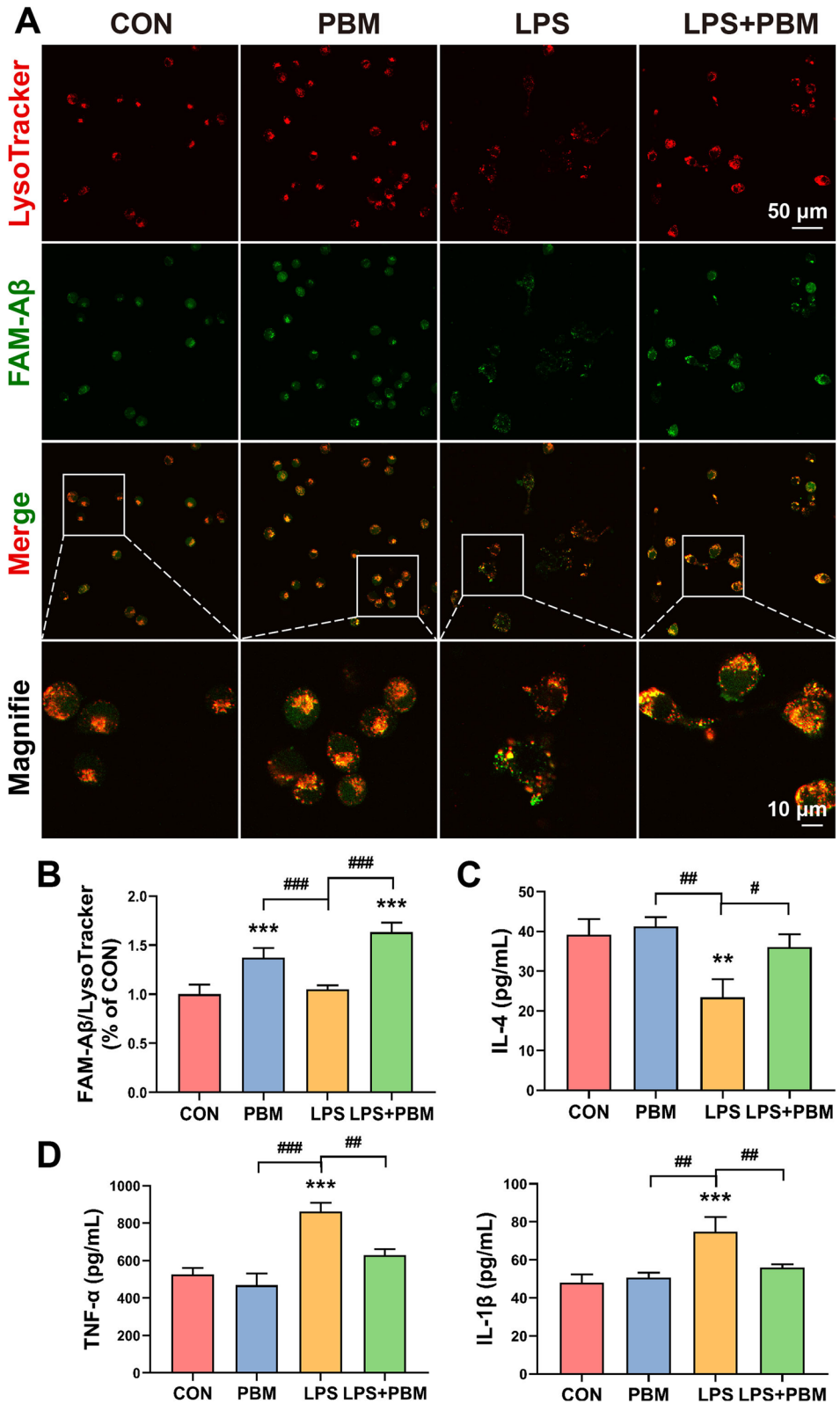

Fig. 9 (See legend on previous page.)

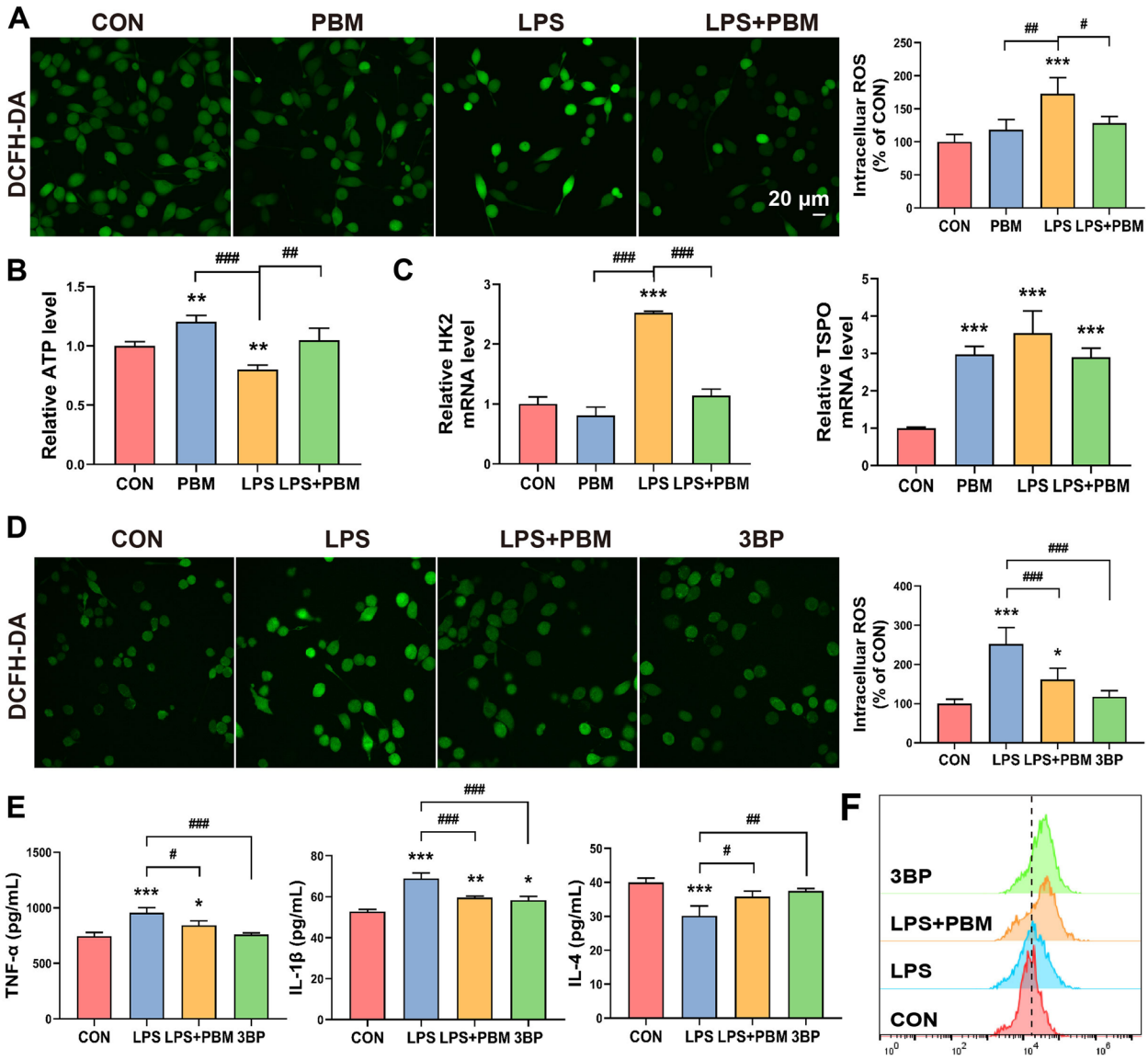

Fig. 10 PBM regulates mitochondrial energy metabolism and microglial phagocytosis by reducing HK2 expression. **A**, **D** Representative images of ROS and quantitative fluorescence intensity of ROS in microglia cultured in vitro. Scale bar: 20 μm. **B** ATP levels in microglia in vitro. (**C**) RT-qPCR analysis of mRNA expression of glycolysis-related genes HK2 and TSPO in microglia. (**E**) Expression levels of pro-inflammatory cytokines TNF-α, IL-1β and anti-inflammatory cytokine IL-4 in the culture supernatant of microglia. **F** Flow cytometry was used to assess the ability of microglia to absorb Aβ. Experimental data are presented as the mean ± standard deviation. Compared with the CON group, $*p < 0.05$, $**p < 0.01$, $***p < 0.001$; Compared with the LPS group, $\#p < 0.05$, $\#\#p < 0.01$, $\#\#\#p < 0.001$

To further substantiate the hypothesis that inhibition of HK2 enhances mitochondrial energy metabolism and improves Aβ phagocytosis in microglia, we assessed the uptake of FAM-$A\beta_{1-42}$ by inflammatory microglia by flow cytometry.

To further substantiate the hypothesis that inhibition of HK2 enhances mitochondrial energy metabolism and improves microglial Aβ phagocytosis, we assessed the uptake capacity of inflammatory microglia for FAM-$A\beta_{1-42}$ by flow cytometry (Fig. 10F). The results demonstrated that the phagocytosis of FAM-$A\beta_{1-42}$

by microglia was substantially enhanced in both the LPS + PBM and 3BP groups compared to that in the LPS group. Consequently, it was demonstrated that PBM treatment could regulate inflammatory cytokine and ROS levels and improve microglial phagocytosis by reducing HK2 expression.

Discussion

AD is a neurodegenerative disease that presents with clinical manifestations, such as progressive memory loss and language dysfunction. These symptoms are primarily due to damage to the brain nerves, which cannot function normally, affecting the daily lives of patients [43]. PBM has been demonstrated to have anti-inflammatory, antioxidant, mitochondrial protective, apoptotic, necrotic inhibitory, and neuroprotective effects [44, 45]. This study demonstrated that PBM was successful in improving neurological damage in APP/PS1 mice following a 6-week PBM intervention in APP/PS1. Further investigation of the mechanism by which PBM exerts its beneficial function revealed that this ameliorative effect might be related to the regulation of mitochondrial energy metabolism by PBM.

Cognitive dysfunction is the principal clinical manifestation of AD [43]. Besides cognitive impairments, such as memory and language deficits, AD is often accompanied by emotional and psychiatric symptoms, including anxiety, depression, hallucinations, and sleep disorders [46]. Furthermore, anxiety and depression-like behaviours have been shown to exacerbate the development of AD [47]. In this study, the MWM and OFT were used to assess cognitive dysfunction and anxiety-like behaviour in mice. The findings of the study demonstrated that the AD group showed diminished memory, whereas the PBM group demonstrated substantially enhanced memory retention for the platform position compared to the AD group following phototherapy. Furthermore, the OFT results indicated that the AD group exhibited diminished capacity for autonomous exploration. However, following PBM treatment, AD mice exhibited active behaviour, increased autonomous exploratory behaviour, and improved anxiety. These findings align with those of other researchers. In a study by Cho et al., PBM was found to alleviate cognitive dysfunction in 5xFAD mice [48]. Yang et al. demonstrated that PBM alleviated anxiety and depressive behaviours in TgF344 rats [49]. Besides cognitive deficits, Aβ accumulation in the brain is the most prominent pathological feature of AD [50]. Several studies have demonstrated that PBM is effective in reducing Aβ accumulation in the brains of individuals with AD [12, 13, 51]. In this study, PBM treatment was found to effectively reduce the number of Aβ plaques in the brains of AD mice, as evidenced by the double-staining result plots of Aβ with the astrocyte marker GFAP. Furthermore, we found that the fluorescence intensity of GFAP was significant reduction around Aβ and in brain tissue, indicating that PBM alleviated AD-induced astrocyte reactivity and reduced inflammatory responses.

Neuroinflammation is one of the causes of AD. Microglia phagocytose Aβ and apoptotic neurons during the early stages of AD pathogenesis to maintain the dynamic equilibrium of amyloid in the brain [52]. However, when Aβ is overproduced, sustained activation of microglia results in a shift from a neuroprotective M2 phenotype to an M1 pro-inflammatory phenotype. This continuous release of pro-inflammatory factors promotes neuroinflammation and triggers neuropathological changes while reducing microglial phagocytosis [53]. This ultimately leads to the development of AD-related dementia [54]. The findings of this study indicate the presence of a considerable number of pro-inflammatory factors in both inflammatory microglia and AD mice. Furthermore, the expression of CD86 was increased, whereas that of Arg-1 was decreased in microglia in an inflammatory environment and in the mouse brain. M1-type microglia are the dominant subtype, and their phagocytic ability is impaired. Consequently, reduction of neuroinflammation may be a therapeutic strategy for AD. Reduced expression of pro-inflammatory factors in AD mice following PBM treatment [55]. In addition, the treatment inhibited the elevated in the levels of pro-inflammatory factors, while promoting the expression of anti-inflammatory factors in AD rats [19]. Furthermore, 810 nm PBM was found to reverse the dominant state of M1 microglia and promote M2 polarisation in the inflammatory environment [56]. Moreover, 1070 nm light can alter the polarisation state of microglia, increase their co-localisation with Aβ, and reduce Aβ plaques aggregation in the brains of AD mice [13]. Similarly, 40 Hz light scintillation therapy effectively promoted phagocytosis in brain microglia and facilitated Aβ clearance [57]. This sparked our desire to explore the potential protective role of PBM in AD. As expected, our results indicate that PBM treatment modulated the expression of inflammatory factors, promoted microglial polarisation towards the M2 phenotype, and strengthened the recruitment and phagocytosis of Aβ by microglia in both an anti-inflammatory milieu and in the brains of AD mice. Consequently, the regulation of microglia to reduce neuroinflammation, reducing Aβ accumulation and clearance, represents a potential therapeutic strategy to treat AD.

The process of programmed cell death that is genetically regulated is called apoptosis. However, in AD, Aβ and neuroinflammation induce excessive neuronal apoptosis, which leads to impaired neuronal loss and

exacerbates the progression of AD [58, 59]. Several studies have demonstrated that Aβ affects the expression of apoptotic proteins, increases mitochondrial membrane permeability, activates caspase proteins, and contributes to apoptosis [60, 61]. This study revealed that the expression of Bax, Caspase3, and Caspase9 in AD was substantially elevated, whereas the expression of Bcl-2 was diminished, and the level of MMP was decreased.. These findings suggest that AD can promote neuronal apoptosis. A previous study demonstrated that PBM inhibits the activation of mitochondria-dependent neuronal apoptosis and exerts neuroprotective effects in hypoxic-ischaemic rats [62]. These findings support the study's results, indicating a significant reduction in pro-apoptotic protein expression in all mice of the PBM group. Moreover, restoration of MMP and elevated Bcl-2 expression were observed. This suggests that PBM inhibits and protects the endogenous apoptotic pathway in the mitochondria of AD neurons.

The stability of mitochondrial energy metabolism is fundamental to the maintenance of normal physiological functions in an organism. NIR PBM is thought to enhance mitochondrial function of stimulated cells by enhancing the activity of cytochrome *c* oxidase (CcO), thereby preventing the degeneration of dopaminergic neurons in Parkinson's patients [63]. One study showed that PBM increases ATP and cAMP (a molecule derived from ATP) by enhancing mitochondrial photoreceptor CcO activity [12]. Cytc, a component of the mitochondrial respiratory chain, plays a role in mitochondrial energy metabolism. CcO and Cytc synergistically participate in the process of cellular respiration and play a key role in the generation of ATP. When the outer mitochondrial membrane is ruptured, Cytc escapes from the mitochondria and activates caspase-9 in the cytoplasm, thereby triggering apoptosis. Our research has found that PBM inhibited AD-induced Cytc release and decreased the Cytc content, thus inhibiting apoptosis.

Mitochondrial oxidative phosphorylation (OXPHOS) and glycolysis are the two main pathways for organisms to obtain ATP, and their intermediate products play an important regulatory role in many cellular life activities [64]. Unlike previous studies, we explored the effects of PBM on mitochondrial OXPHOS and glycolysis in AD. Among these, OXPHOS is closely related to apoptosis, and the occurrence of apoptosis is associated with an impaired reduction in OXPHOS [65, 66]. Conversely, aberrant mitochondrial function results in reduced OXPHOS levels in AD, with glycolysis representing the principal pathway of energy metabolism [67]. PGC-1α is a key transcriptional coactivator that regulates mitochondrial function and determines many mitochondrial functions, including respiration, biogenesis, and redox [68, 69]. PGC-1α also induces and binds to NRF-1, enhancing mitochondrial OXPHOS [70]. In contrast, the glycolytic pathway primarily produces ATP from glucose, which is mediated by GLUT, HK2, and pyruvate kinase [71]. Through experiments, we observed that the expression of PGC-1α and NRF-1 in the brain of APP/PS1 mice was significantly reduced, and the expression levels of GLUT1, PKM2 and HK2 were increased. This suggests that AD leads to a shift in neuronal mitochondrial energy metabolism from OXPHOS to glycolysis. And after phototherapy, PBM was found to be effective in reversing this phenomenon, inhibiting glycolysis and promoting OXPHOS. The experimental results showed that PBM can inhibit neuronal apoptosis by regulating mitochondrial metabolism and promoting OXPHOS, preventing Cytc release.

AD microglia require considerable energy to phagocytose Aβ. A strong positive correlation was observed between increased ATP levels resulting from the microglial OXPHOS pathway and enhanced Aβ phagocytosis [28]. In the event of Aβ accumulation, an increase in glycolysis at the expense of OXPHOS in the inflammatory states results in a deficiency of energy production in microglia [72], as well as the generation of excessive ROS, which causes oxidative damage and cytotoxicity [73]. These results demonstrated that PBM increased ATP levels and reduced ROS levels in LPS-induced microglia, promoting energy metabolism and enhancing microglial phagocytosis. In microglia of 5xFAD mice and AD patients, the expression of HK2 is specifically elevated [74]. This results in the conversion of pro-inflammatory microglia to oxidative respiration and glycolysis, which accelerate the development of inflammation [75]. The results demonstrated that HK2 expression was markedly elevated in both the inflammatory milieu and brains of AD mice. Furthermore, PBM substantially reduced the levels of HK2 during glycolysis and enhanced the mitochondrial energy metabolism. Moreover, there is an interactive relationship between the activity of the glycolytic enzyme HK2 and microglial phagocytosis in AD [76]. Pharmacological inhibition of HK2 can promote microglial phagocytosis and improve memory impairment in AD mice [74]. In addition, HK2 knockdown inhibits microglia-mediated neuroinflammation [77]. The HK2 inhibitor 3BP was used, and it was observed that both 3BP and PBM treatment reduced ROS content, improved inflammatory factor expression in cells, attenuated neuroinflammation, and promoted the ability of microglia to phagocytose Aβ. Consequently, it has been postulated that PBM treatment may promote microglial phagocytosis, reduce neuroinflammation, and improve AD by inhibiting HK2 expression.

In addition to the AD in this study, PBM can be used to treat other neurodegenerative diseases such as Parkinson's [78], stroke [79], and epilepsy [80]. And PBM has been shown to be useful for the treatment of eye diseases [18] and bone injury repair [81]. Future research on PBM therapy can focus on the following areas. In the study of PBM treatment of ophthalmic diseases, it is necessary to optimize the treatment parameters and explore the long-term efficacy and safety. In terms of immune system diseases, the specific mechanism and efficacy of its regulation of immune function should be clarified. In the treatment of tumors, it is necessary to study how light affects the tumor microenvironment and immune cell function. The application prospects of PBM therapy are very broad. However, its clinical application is still limited. We describe this in the "Limitation" section.

Limitation

Studies have shown that NIR transcranial PBM has a relatively strong transmittance through the mouse skull (8%−25%) [13, 29]. Therefore, when we performed in vivo experiments, we performed 808 nm NIR intervention on AD mice after shaving their heads. Our experimental results confirmed that PBM was able to improve AD pathology in mice. However, the transmission of transcranial NIR through thicker human skulls is extremely low, which is an important obstacle to its clinical translation. In addition to this, the effects of microglia on Aβ may be multifaceted, and in this study we only focused on their phagocytic ability to Aβ and the effects of their polarization state on neuroinflammation. Therefore, there is insufficient evidence to confirm that PBM affects microglia to directly alleviate cognitive deficits and improve AD pathology. Further research is needed on the specific molecular mechanism and clinical application of PBM in the treatment of AD.

Conclusion

Our results confirm that PBM can improve cognitive impairment and neurological damage in AD mice. In addition, we found that PBM can restore mitochondrial energy metabolism, promote oxidative phosphorylation, inhibit glycolysis, and improve mitophagic dysbiosis. This helps to inhibit neuronal apoptosis and regulate microglial polarization, thereby reducing Aβ burden and alleviating pathology in AD mice. This work provides valuable insights into the therapeutic effect and underlying mechanism of PBM on AD.

Abbreviations

AD	Alzheimer's disease
Aβ	Amyloid β-protein
PBM	Photobiomodulation
LPS	Lipopolysaccharide
HK2	Hexokinase 2
3BP	3-Bromopyruvate
Cytc	Cytochrome C
CNS	Central nervous system
APP	Amyloid precursor protein
MLCs	Mitochondria-lysosomal contacts
ROS	Reactive oxygen species
OXPHOS	Oxidative phosphorylation
NIR	Near-infrared
CON	Control
MWM	Morris water maze
OFT	Open-field test
PBS	Phosphate-buffered saline
PFA	Paraformaldehyde
GFAP	Gnti-glial fibrillary acidic protein
HE	Haematoxylin and eosin
ELISA	Enzyme-linked immunosorbent assay
MMP	Mitochondrial membrane potential
RT-PCR	Reverse transcription polymerase chain reaction
WB	Western blotting
MCC	Manders' Colocalization Coefficients
IL-4	Interleukin-4
TNF-α	Tumour necrosis factor-α
NLRP3	The Nod-like receptor protein 3
PGC-1α	Peroxisome proliferator-activated receptor-γ coactivator-1α
NRF-1	Nuclear respiratory factor
GLUT1	Glucose transporter protein 1
CcO	Cytochrome c oxidase

Supplementary Information

The online version contains supplementary material available at https://doi.org/10.1186/s13195-025-01714-w.

Supplementary Material 1: Source data 1. In Fig. 3, the unedited blots and figures with the uncropped blots with the relevant bands clearly labeled.

Supplementary Material 2: Source data 2. In Fig. 5, the unedited blots and figures with the uncropped blots with the relevant bands clearly labeled.

Supplementary Material 3: Source data 3. In Fig. 6, the unedited blots and figures with the uncropped blots with the relevant bands clearly labeled.

Supplementary Material 4: Source data 4. In Fig. 7, the unedited blots and figures with the uncropped blots with the relevant bands clearly labeled.

Supplementary Material 5: Supplementary Fig. 1. ELISA was used to detect the expression of apoptosis factors. The expressions of apoptosis factors Bcl-2 (A), Bax (B), Caspsae3 (C) and Caspase9 (D) were detected by ELISA, and the effects of PBM on apoptosis related proteins of AD nerve cells were investigated. Compared with the CON group, $^{**}p < 0.01$, $^{***}p < 0.001$; Compared with the LPS group, $\#p < 0.05$, $\#\#p < 0.01$, $\#\#\#p < 0.001$.

Acknowledgements

We would like to thank Figdraw (the assistance in creating figures. www.figdraw.com) for the assistance in creating figures.

Authors' contributions

H. C., X. W. and H. Y. designed the overall study and revised the paper. N. L., N. L., and H. Z. carried out experiments, collected, analysed data, and writing – original draft. C. M., Y. Y. and X. S. collected, analysed data, and co-wrote the paper. G. L., X. D. and T. T. revised the paper. All authors reviewed and approved the final version of the manuscript.

Funding

This work was supported by the Natural Science Foundation of Hebei Province, No. F2024110001 (to HC); the National Natural Science Foundation of China, Nos. 62175261 (to HY) and 82471536 (to TT); the National Key R&D Program of China Nos. 2023YFC2412502 and 2023YFB3609103 (to HY); the Chinese Academy of Medical Sciences Innovation Fund for Medical Sciences, No. 2021-I2M-1–058 (to HY); and the Oujiang Laboratory, No. OJQD2022002

and Wenzhou Science and Technology Projects, Nos. 2023ZM006 and 2024R2002 (to TT).

Data availability
Data is provided within the manuscript or supplementary information files.

Declarations

Ethics approval and consent to participate
The Animal Care and Experimental Program was approved by the Institute of Radiological Medicine, Chinese Academy of Medical Sciences (ethical review No. IRM-DWLL-2023017).

Consent for publication
Not applicable.

Competing interests
The authors declare no competing interests.

Author details
[1]State Key Laboratory of Advanced Medical Materials and Devices, Tianjin Key Laboratory of Neuromodulation and Neurorepair, Integrative Regeneration Laboratory, Institute of Biomedical Engineering, Chinese Academy of Medical Sciences & Peking Union Medical College, Tianjin 300192, China. [2]State Key Laboratory of Separation Membranes and Membrane Processes & Key Laboratory of Hollow Fiber Membrane Materials and Membrane Processes, Tianjin Key Laboratory of Optoelectronic Detection Technology and Systems, School of Life Sciences, Tiangong University, Tianjin 300387, China. [3]Cangzhou Institute of Tiangong University, Cangzhou 061000, China. [4]Institute of Mental Health, Tianjin Anding Hospital, Mental Health Center of Tianjin Medical University, Tianjin 300222, China. [5]Oujiang Laboratory (Zhejiang Lab for Regenerative Medicine, Vision and Brain Health), Institute of Aging, Key Laboratory of Alzheimer's Disease of Zhejiang Province, Zhejiang Provincial Clinical Research Center for Mental Disorders, The Affiliated Wenzhou Kangning Hospital, Wenzhou Medical University, Wenzhou, Zhejiang, P.R. 325000, China. [6]Key Laboratory of Carcinogenesis and Translational Research (Ministry of Education/Beijing), Cancer Hospital & Institute, International Cancer Institute, Institute of Medical Technology, Peking University Health Science Center, Biomedical Engineering Department, Peking University, Beijing 100142, China.

Received: 28 November 2024 Accepted: 10 March 2025
Published online: 05 April 2025

References

1. Xiao M, Xiang W, Chen Y, Peng N, Du X, Lu S, Zuo Y, Li B, Hu Y, Li X. DHA Ameliorates Cognitive Ability, Reduces Amyloid Deposition, and Nerve Fiber Production in Alzheimer's Disease. Front Nutr. 2022;9: 852433.
2. Zhang Y, Chen H, Li R, Sterling K, Song W. Amyloid β-based therapy for Alzheimer's disease: challenges, successes and future. Signal Transduct Target Ther. 2023;8(1):248.
3. Congdon EE, Ji C, Tetlow AM, Jiang Y, Sigurdsson EM. Tau-targeting therapies for Alzheimer disease: current status and future directions. Nat Rev Neurol. 2023;19(12):715–36.
4. Menzie J, Pan C, Prentice H, Wu JY. Taurine and central nervous system disorders. Amino Acids. 2014;46(1):31–46.
5. Mathys H, Peng Z, Boix CA, Victor MB, Leary N, Babu S, Abdelhady G, Jiang X, Ng AP, Ghafari K, et al. Single-cell atlas reveals correlates of high cognitive function, dementia, and resilience to Alzheimer's disease pathology. Cell. 2023;186(20):4365-4385.e4327.
6. Li Y, Liu Q, Sun J, Wang J, Liu X, Gao J. Mitochondrial protective mechanism of simvastatin protects against amyloid β peptide-induced injury in SH-SY5Y cells. Int J Mol Med. 2018;41(5):2997–3005.
7. Koenigsknecht-Talboo J, Landreth GE. Microglial phagocytosis induced by fibrillar beta-amyloid and IgGs are differentially regulated by proinflammatory cytokines. J Neurosci. 2005;25(36):8240–9.
8. Dhapola R, Hota SS, Sarma P, Bhattacharyya A, Medhi B, Reddy DH. Recent advances in molecular pathways and therapeutic implications targeting neuroinflammation for Alzheimer's disease. Inflammopharmacology. 2021;29(6):1669–81.
9. de Freitas LF, Hamblin MR. Proposed Mechanisms of Photobiomodulation or Low-Level Light Therapy. IEEE J Sel Top Quantum Electron. 2016;22(3):7000417.
10. Golovynska I, Golovynskyi S, Stepanov YV, Stepanova LI, Qu J, Ohulchanskyy TY. Red and near-infrared light evokes Ca^{2+} influx, endoplasmic reticulum release and membrane depolarization in neurons and cancer cells. J Photochem Photobiol B. 2021;214: 112088.
11. Renlong Z, Ting Z, Liwei L, Tymish YO, Junle Q. Dose–effect relationships for PBM in the treatment of Alzheimer's disease. J Phys D: Appl Phys. 2021;54(35): 353001.
12. Zhang Z, Shen Q, Wu X, Zhang D, Xing D. Activation of PKA/SIRT1 signaling pathway by photobiomodulation therapy reduces Aβ levels in Alzheimer's disease models. Aging Cell. 2020;19(1): e13054.
13. Tao L, Liu Q, Zhang F, Fu Y, Zhu X, Weng X, Han H, Huang Y, Suo Y, Chen L, et al. Microglia modulation with 1070-nm light attenuates Aβ burden and cognitive impairment in Alzheimer's disease mouse model. Light Sci Appl. 2021;10(1):179.
14. Chen C, Bao Y, Xing L, Jiang C, Guo Y, Tong S, Zhang J, Chen L, Mao Y. Exosomes Derived from M2 Microglial Cells Modulated by 1070-nm Light Improve Cognition in an Alzheimer's Disease Mouse Model. Adv Sci (Weinh). 2023;10(32): e2304025.
15. Qiu K, Zou W, Fang H, Hao M, Mehta K, Tian Z, Guan JL, Zhang K, Huang T, Diao J. Light-activated mitochondrial fission through optogenetic control of mitochondria-lysosome contacts. Nat Commun. 2022;13(1):4303.
16. Eells JT, Wong-Riley MT, VerHoeve J, Henry M, Buchman EV, Kane MP, Gould LJ, Das R, Jett M, Hodgson BD, et al. Mitochondrial signal transduction in accelerated wound and retinal healing by near-infrared light therapy. Mitochondrion. 2004;4(5–6):559–67.
17. Begum R, Calaza K, Kam JH, Salt TE, Hogg C and Jeffery G. Near-infrared light increases ATP, extends lifespan and improves mobility in aged Drosophila melanogaster. Biol Lett. 2015;11(3):20150073.
18. El Massri N, Weinrich TW, Kam JH, Jeffery G, Mitrofanis J. Photobiomodulation reduces gliosis in the basal ganglia of aged mice. Neurobiol Aging. 2018;66:131–7.
19. Yang L, Wu C, Parker E, Li Y, Dong Y, Tucker L, Brann DW, Lin HW, Zhang Q. Non-invasive photobiomodulation treatment in an Alzheimer Disease-like transgenic rat model. Theranostics. 2022;12(5):2205–31.
20. Chakravorty A, Jetto CT, Manjithaya R. Dysfunctional Mitochondria and Mitophagy as Drivers of Alzheimer's Disease Pathogenesis. Front Aging Neurosci. 2019;11:311.
21. Swerdlow RH. Mitochondria and Mitochondrial Cascades in Alzheimer's Disease. J Alzheimers Dis. 2018;62(3):1403–16.
22. Liang J, Wang C, Zhang H, Huang J, Xie J, Chen N. Exercise-Induced Benefits for Alzheimer's Disease by Stimulating Mitophagy and Improving Mitochondrial Function. Front Aging Neurosci. 2021;13: 755665.
23. Farsi RM. The Role of Mitochondrial Dysfunction in Alzheimer's: Molecular Defects and Mitophagy-Enhancing Approaches. Life (Basel). 2023;13(4):970.
24. Hu Y, Cao K, Wang F, Wu W, Mai W, Qiu L, Luo Y, Ge WP, Sun B, Shi L, et al. Dual roles of hexokinase 2 in shaping microglial function by gating glycolytic flux and mitochondrial activity. Nat Metab. 2022;4(12):1756–74.
25. Zhou F, Lian W, Yuan X, Wang Z, Xia C, Yan Y, Wang W, Tong Z, Cheng Y, Xu J, et al. Cornuside alleviates cognitive impairments induced by Aβ1−42 through attenuating NLRP3-mediated neurotoxicity by promoting mitophagy. Alzheimer's Research & Therapy. 2025;17(1):47.
26. Ma KG, Lv J, Yang WN, Chang KW, Hu XD, Shi LL, Zhai WY, Zong HF, Qian YH. The p38 mitogen activated protein kinase regulates β-amyloid protein internalization through the α7 nicotinic acetylcholine receptor in mouse brain. Brain Res Bull. 2018;137:41–52.
27. Alberdi E, Sánchez-Gómez MV, Ruiz A, Cavaliere F, Ortiz-Sanz C, Quintela-López T, Capetillo-Zarate E, Solé-Domènech S, Matute C. Mangiferin and Morin Attenuate Oxidative Stress, Mitochondrial Dysfunction, and Neurocytotoxicity, Induced by Amyloid Beta Oligomers. Oxid Med Cell Longev. 2018;2018:2856063.
28. Li Q, Peng J, Luo Y, Zhou J, Li T, Cao L, Peng S, Zuo Z, Wang Z. Far infrared light irradiation enhances Aβ clearance via increased exocytotic

microglial ATP and ameliorates cognitive deficit in Alzheimer's disease-like mice. J Neuroinflammation. 2022;19(1):145.
29. Wang M, Yan C, Li X, Yang T, Wu S, Liu Q, Luo Q, Zhou F. Non-invasive modulation of meningeal lymphatics ameliorates ageing and Alzheimer's disease-associated pathology and cognition in mice. Nat Commun. 2024;15(1):1453.
30. Richard BC, Kurdakova A, Baches S, Bayer TA, Weggen S, Wirths O. Gene Dosage Dependent Aggravation of the Neurological Phenotype in the 5XFAD Mouse Model of Alzheimer's Disease. J Alzheimers Dis. 2015;45(4):1223–36.
31. Minkeviciene R, Ihalainen J, Malm T, Matilainen O, Keksa-Goldsteine V, Goldsteins G, Iivonen H, Leguit N, Glennon J, Koistinaho J, et al. Age-related decrease in stimulated glutamate release and vesicular glutamate transporters in APP/PS1 transgenic and wild-type mice. J Neurochem. 2008;105(3):584–94.
32. Jackson HM, Soto I, Graham LC, Carter GW, Howell GR. Clustering of transcriptional profiles identifies changes to insulin signaling as an early event in a mouse model of Alzheimer's disease. BMC Genomics. 2013;14:831.
33. Mariscal P, Bravo L, Llorca-Torralba M, Razquin J, Miguelez C, Suárez-Pereira I, Berrocoso E. Sexual differences in locus coeruleus neurons and related behavior in C57BL/6J mice. Biol Sex Differ. 2023;14(1):64.
34. Ma C, Zhu H, Cai Y, Li N, Han Z, Wu H and Chen H. Photobiomodulation Combined With Human Umbilical Cord Mesenchymal Stem Cells Modulates the Polarization of Microglia. J Biophotonics. 2025:e202400468.
35. Rafaella Carvalho R, Gilles S, Aníbal A, Cristina PS. Photobiomodulation in human neuroblastoma under oxidative stress. Alzheimer's Dement. 2023;19: e063129.
36. Tamagno E, Guglielmotto M, Monteleone D, Manassero G, Vasciaveo V, Tabaton M. The Unexpected Role of Aβ1-42 Monomers in the Pathogenesis of Alzheimer's Disease. J Alzheimers Dis. 2018;62(3):1241–5.
37. Alemi M, Gaiteiro C, Ribeiro CA, Santos LM, Gomes JR, Oliveira SM, Couraud PO, Weksler B, Romero I, Saraiva MJ, et al. Transthyretin participates in beta-amyloid transport from the brain to the liver–involvement of the low-density lipoprotein receptor-related protein 1? Sci Rep. 2016;6:20164.
38. Fleisher-Berkovich S, Filipovich-Rimon T, Ben-Shmuel S, Hülsmann C, Kummer MP, Heneka MT. Distinct modulation of microglial amyloid β phagocytosis and migration by neuropeptides (i). J Neuroinflammation. 2010;7:61.
39. Serrano-Pozo A, Li H, Li Z, Muñoz-Castro C, Jaisa-Aad M, Healey MA, Welikovitch LA, Jayakumar R, Bryant AG, Noori A, et al. Astrocyte transcriptomic changes along the spatiotemporal progression of Alzheimer's disease. Nat Neurosci. 2024;27(12):2384–400.
40. Escartin C, Galea E, Lakatos A, O'Callaghan JP, Petzold GC, Serrano-Pozo A, Steinhäuser C, Volterra A, Carmignoto G, Agarwal A, et al. Reactive astrocyte nomenclature, definitions, and future directions. Nat Neurosci. 2021;24(3):312–25.
41. Dong Y, Li S, Lu Y, Li X, Liao Y, Peng Z, Li Y, Hou L, Yuan Z, Cheng J. Stress-induced NLRP3 inflammasome activation negatively regulates fear memory in mice. J Neuroinflammation. 2020;17(1):205.
42. Mallach A, Zielonka M, van Lieshout V, An Y, Khoo JH, Vanheusden M, Chen WT, Moechars D, Arancibia-Carcamo IL, Fiers M, et al. Microglia-astrocyte crosstalk in the amyloid plaque niche of an Alzheimer's disease mouse model, as revealed by spatial transcriptomics. Cell Rep. 2024;43(6): 114216.
43. Pisani S, Mueller C, Huntley J, Aarsland D, Kempton MJ. A meta-analysis of randomised controlled trials of physical activity in people with Alzheimer's disease and mild cognitive impairment with a comparison to donepezil. Int J Geriatr Psychiatry. 2021;36(10):1471–87.
44. Zhou T, Ohulchanskyy TY, Qu J. Effect of NIR light on the permeability of the blood-brain barriers in in vitro models. Biomed Opt Express. 2021;12(12):7544–55.
45. Bathini M, Raghushaker CR, Mahato KK. The Molecular Mechanisms of Action of Photobiomodulation Against Neurodegenerative Diseases: A Systematic Review. Cell Mol Neurobiol. 2022;42(4):955–71.
46. Sabates J, Chiu WH, Loi S, Lampit A, Gavelin HM, Chong T, Launder N, Goh AMY, Brodtmann A, Lautenschlager N, et al. The Associations Between Neuropsychiatric Symptoms and Cognition in People with Dementia: A Systematic Review and Meta-Analysis. Neuropsychol Rev. 2024;34(2):581–97.
47. Burke SL, Cadet T, Alcide A, O'Driscoll J, Maramaldi P. Psychosocial risk factors and Alzheimer's disease: the associative effect of depression, sleep disturbance, and anxiety. Aging Ment Health. 2018;22(12):1577–84.
48. Cho GM, Lee SY, Park JH, Kim MJ, Park KJ, Choi BT, Shin YI, Kim NG, Shin HK. Photobiomodulation Using a Low-Level Light-Emitting Diode Improves Cognitive Dysfunction in the 5XFAD Mouse Model of Alzheimer's Disease. J Gerontol A Biol Sci Med Sci. 2020;75(4):631–9.
49. Yang L, Wu C, Tucker L, Dong Y, Li Y, Xu P, Zhang Q. Photobiomodulation Therapy Attenuates Anxious-Depressive-Like Behavior in the TgF344 Rat Model. J Alzheimers Dis. 2021;83(4):1415–29.
50. Rahman MM, Lendel C. Extracellular protein components of amyloid plaques and their roles in Alzheimer's disease pathology. Mol Neurodegener. 2021;16(1):59.
51. Zinchenko E, Navolokin N, Shirokov A, Khlebtsov B, Dubrovsky A, Saranceva E, Abdurashitov A, Khorovodov A, Terskov A, Mamedova A, et al. Pilot study of transcranial photobiomodulation of lymphatic clearance of beta-amyloid from the mouse brain: breakthrough strategies for non-pharmacologic therapy of Alzheimer's disease. Biomed Opt Express. 2019;10(8):4003–17.
52. Durafourt BA, Moore CS, Blain M, Antel JP. Isolating, culturing, and polarizing primary human adult and fetal microglia. Methods Mol Biol. 2013;1041:199–211.
53. Pan XD, Zhu YG, Lin N, Zhang J, Ye QY, Huang HP, Chen XC. Microglial phagocytosis induced by fibrillar β-amyloid is attenuated by oligomeric β-amyloid: implications for Alzheimer's disease. Mol Neurodegener. 2011;6:45.
54. Lučiūnaitė A, McManus RM, Jankunec M, Rácz I, Dansokho C, Dalgėdienė I, Schwartz S, Brosseron F, Heneka MT. Soluble Aβ oligomers and protofibrils induce NLRP3 inflammasome activation in microglia. J Neurochem. 2020;155(6):650–61.
55. De Taboada L, Yu J, El-Amouri S, Gattoni-Celli S, Richieri S, McCarthy T, Streeter J, Kindy MS. Transcranial laser therapy attenuates amyloid-β peptide neuropathology in amyloid-β protein precursor transgenic mice. J Alzheimers Dis. 2011;23(3):521–35.
56. Song JW, Li K, Liang ZW, Dai C, Shen XF, Gong YZ, Wang S, Hu XY, Wang Z. Low-level laser facilitates alternatively activated macrophage/microglia polarization and promotes functional recovery after crush spinal cord injury in rats. Sci Rep. 2017;7(1):620.
57. Singer AC, Martorell AJ, Douglas JM, Abdurrob F, Attokaren MK, Tipton J, Mathys H, Adaikkan C, Tsai LH. Noninvasive 40-Hz light flicker to recruit microglia and reduce amyloid beta load. Nat Protoc. 2018;13(8):1850–68.
58. Sharma VK, Singh TG, Singh S, Garg N, Dhiman S. Apoptotic Pathways and Alzheimer's Disease: Probing Therapeutic Potential. Neurochem Res. 2021;46(12):3103–22.
59. Ekundayo BE, Obafemi TO, Adewale OB, Obafemi BA, Oyinloye BE, Ekundayo SK. Oxidative Stress, Endoplasmic Reticulum Stress and Apoptosis in the Pathology of Alzheimer's Disease. Cell Biochem Biophys. 2024;82(2):457–77.
60. Kudo W, Lee HP, Smith MA, Zhu X, Matsuyama S, Lee HG. Inhibition of Bax protects neuronal cells from oligomeric Aβ neurotoxicity. Cell Death Dis. 2012;3(5): e309.
61. Bandaru LJM, Ayyalasomayajula N, Murumulla L, Challa S. Mechanisms associated with the dysregulation of mitochondrial function due to lead exposure and possible implications on the development of Alzheimer's disease. Biometals. 2022;35(1):1–25.
62. Tucker LD, Lu Y, Dong Y, Yang L, Li Y, Zhao N, Zhang Q. Photobiomodulation Therapy Attenuates Hypoxic-Ischemic Injury in a Neonatal Rat Model. J Mol Neurosci. 2018;65(4):514–26.
63. Foo ASC, Soong TW, Yeo TT, Lim KL. Mitochondrial Dysfunction and Parkinson's Disease-Near-Infrared Photobiomodulation as a Potential Therapeutic Strategy. Front Aging Neurosci. 2020;12:89.
64. Cao J, Li M, Liu K, Shi X, Sui N, Yao Y, Wang X, Li S, Tian Y, Tan S, et al. Oxidative phosphorylation safeguards pluripotency via UDP-N-acetylglucosamine. Protein Cell. 2023;14(5):376–81.
65. Yamaguchi N, Kieba IR, Korostoff J, Howard PS, Shenker BJ, Lally ET. Maintenance of oxidative phosphorylation protects cells from Actinobacillus actinomycetemcomitans leukotoxin-induced apoptosis. Cell Microbiol. 2001;3(12):811–23.
66. Peng X, Gan J, Wang Q, Shi Z, Xia X. 3-Monochloro-1,2-propanediol (3-MCPD) induces apoptosis via mitochondrial oxidative phosphorylation

system impairment and the caspase cascade pathway. Toxicology. 2016;372:1–11.
67. Bordone MP, Salman MM, Titus HE, Amini E, Andersen JV, Chakraborti B, Diuba AV, Dubouskaya TG, Ehrke E, Espindola de Freitas A, et al. The energetic brain - A review from students to students. J Neurochem. 2019;151(2):139–165.
68. Sun X, Liu X, Yu K, Xu S, Qiu P, Lv Z, Zhang X, Xu Y. Targeting PGC1α to wrestle cancer: a compelling therapeutic opportunity. J Cancer Res Clin Oncol. 2022;148(4):767–74.
69. Finck BN, Kelly DP. PGC-1 coactivators: inducible regulators of energy metabolism in health and disease. J Clin Invest. 2006;116(3):615–22.
70. Schank M, Zhao J, Wang L, Li Z, Cao D, Nguyen LN, Dang X, Khanal S, Nguyen LNT, Thakuri BKC, et al. Telomeric injury by KML001 in human T cells induces mitochondrial dysfunction through the p53-PGC-1α pathway. Cell Death Dis. 2020;11(12):1030.
71. Chandel NS. Glycolysis. Cold Spring Harb Perspect Biol. 2021;13(5):a040535.
72. Serio S, Pagiatakis C, Musolino E, Felicetta A, Carullo P, Laura Frances J, Papa L, Rozzi G, Salvarani N, Miragoli M, et al. Cardiac Aging Is Promoted by Pseudohypoxia Increasing p300-Induced Glycolysis. Circ Res. 2023;133(8):687–703.
73. Boese AC, Kang S. Mitochondrial metabolism-mediated redox regulation in cancer progression. Redox Biol. 2021;42: 101870.
74. Leng L, Yuan Z, Pan R, Su X, Wang H, Xue J, Zhuang K, Gao J, Chen Z, Lin H, et al. Microglial hexokinase 2 deficiency increases ATP generation through lipid metabolism leading to β-amyloid clearance. Nat Metab. 2022;4(10):1287–305.
75. Hu Y, Mai W, Chen L, Cao K, Zhang B, Zhang Z, Liu Y, Lou H, Duan S, Gao Z. mTOR-mediated metabolic reprogramming shapes distinct microglia functions in response to lipopolysaccharide and ATP. Glia. 2020;68(5):1031–45.
76. Choi H, Mook-Jung I. Lipid fuel for hungry-angry microglia. Nat Metab. 2022;4(10):1223–4.
77. Li Y, Lu B, Sheng L, Zhu Z, Sun H, Zhou Y, Yang Y, Xue D, Chen W, Tian X, et al. Hexokinase 2-dependent hyperglycolysis driving microglial activation contributes to ischemic brain injury. J Neurochem. 2018;144(2):186–200.
78. Boaz K, John M, Jonathan S, Daniel MJ. Remote tissue conditioning is neuroprotective against MPTP insult in mice. IBRO Reports. 2018;4:14–7.
79. Margaret AN, Michael H, Paula IM, Michael RH, Bang-Bon K. Increased Functional Connectivity Within Intrinsic Neural Networks in Chronic Stroke Following Treatment with Red/Near-Infrared Transcranial Photobiomodulation: Case Series with Improved Naming in Aphasia. Photobiomodulation Photomed Laser Surg. 2020;38:115–31.
80. Nasr MR, Naglaa AA, Khayria Mansour I, Mona Emam K, Mona AEA, Yasser AK. Effect of Infrared Laser Irradiation on Amino Acid Neurotransmitters in an Epileptic Animal Model Induced by Pilocarpine. Photomed Laser Surg. 2009;27:401–9.
81. Lu P, Peng J, Liu J, Chen L. The role of photobiomodulation in accelerating bone repair. Prog Biophys Mol Biol. 2024;188:55–67.

Publisher's Note